# Systemic inflammatory response syndrome triggered by blood-borne pathogens induces prolonged dendritic cell paralysis and immunosuppression

Mitra Ashayeripanah, Javier Vega-Ramos, Daniel Fernandez-Ruiz, Shirin Valikhani, Aaron T.L. Lun, Jason White, Louise Young, Atefeh Yaftiyan, Yifan Zhan, Linda Wakim, et al.

Article

Cell Reports

# Systemic inflammatory response syndrome triggered by blood-borne pathogens induces prolonged dendritic cell paralysis and immunosuppression

## Graphical abstract

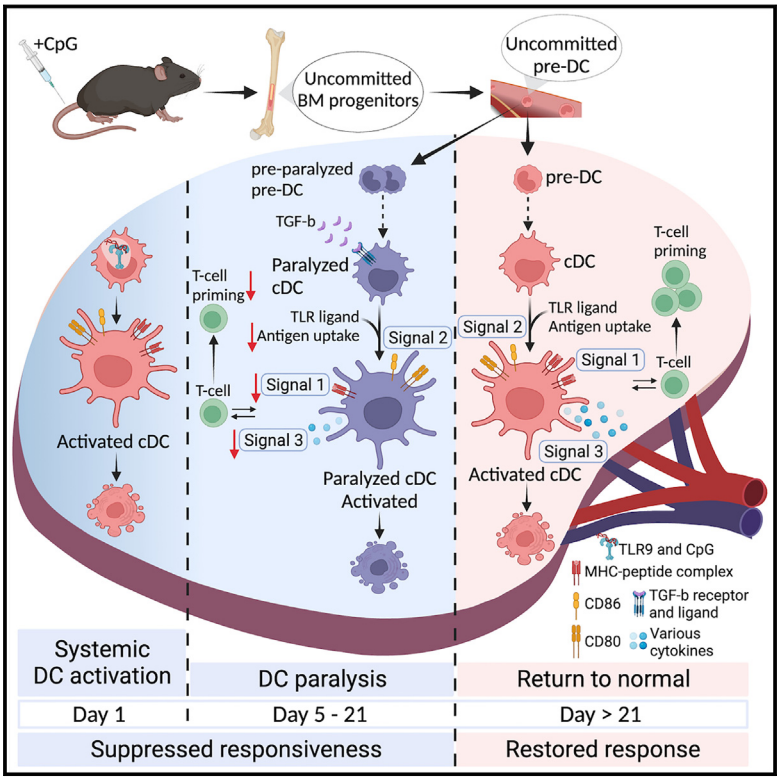


## Highlights

- Blood infections cause severe inflammation followed by protracted immunosuppression
- Impaired immunity is due to formation of paralyzed conventional dendritic cells (cDCs)
- Local secondary signals that persist after resolution of infection induce paralysis
- Therapies that overcome or reduce the duration of cDC paralysis restore immunocompetence

## Authors

Mitra Ashayeripanah, Javier Vega-Ramos, Daniel Fernandez-Ruiz, ..., Justine D. Mintern, Antoine Roquilly, Jose A. Villadangos

## Correspondence

antoine.roquilly@chu-nantes.fr (A.R.), j.villadangos@unimelb.edu.au (J.A.V.)

## In brief

Ashayeripanah et al. show that severe inflammation triggered by blood infections such as malaria induces formation of functionally impaired (paralyzed) dendritic cells for weeks after resolution of infection. Paralysis causes immune suppression. Transcriptomic, phenotypic, and functional characterization of paralysis leads to designing treatments that restore dendritic cell function and immunocompetence.

Ashayeripanah et al., 2024, Cell Reports *43*, 113754
February 27, 2024 
https://doi.org/10.1016/j.celrep.2024.113754

CellPress

Cell Reports

CellPress
OPEN ACCESS

Article

# Systemic inflammatory response syndrome triggered by blood-borne pathogens induces prolonged dendritic cell paralysis and immunosuppression

Mitra Ashayeripanah,[1] Javier Vega-Ramos,[1,2] Daniel Fernandez-Ruiz,[1,3] Shirin Valikhani,[1] Aaron T.L. Lun,[2,4] Jason T. White,[1] Louise J. Young,[2,4] Atefeh Yaftiyan,[1] Yifan Zhan,[2,4] Linda Wakim,[1] Irina Caminschi,[5] Mireille H. Lahoud,[5] Andrew M. Lew,[2,4] Ken Shortman,[2,4] Gordon K. Smyth,[2,6] William R. Heath,[1] Justine D. Mintern,[2,7] Antoine Roquilly,[1,8,9,*] and Jose A. Villadangos[1,7,10,*]

[1]Department of Microbiology and Immunology, Peter Doherty Institute for Infection and Immunity, The University of Melbourne, Parkville, VIC 3000, Australia
[2]The Walter and Eliza Hall Institute of Medical Research, Parkville, VIC 3052, Australia
[3]School of Biomedical Sciences, Faculty of Medicine & Health and the UNSW RNA Institute, The University of New South Wales, Kensington, NSW 2052, Australia
[4]Department of Medical Biology, The University of Melbourne, Parkville, VIC 3010, Australia
[5]Immunity Program, Monash Biomedicine Discovery Institute and Department of Biochemistry and Molecular Biology, Monash University, Clayton, VIC 3800, Australia
[6]Department of Mathematics and Statistics, The University of Melbourne, Parkville, VIC 3010, Australia
[7]Department of Biochemistry and Pharmacology, Bio21 Molecular Science and Biotechnology Institute, The University of Melbourne, Parkville, VIC 3010, Australia
[8]Nantes Université, CHU Nantes, INSERM, Center for Research in Transplantation and Translational Immunology, UMR 1064, 44000 Nantes, France
[9]CHU Nantes, INSERM, Nantes Université, Anesthesie Reanimation, CIC 1413, 44000 Nantes, France
[10]Lead contact
*Correspondence: antoine.roquilly@chu-nantes.fr (A.R.), j.villadangos@unimelb.edu.au (J.A.V.)
https://doi.org/10.1016/j.celrep.2024.113754

## SUMMARY

Blood-borne pathogens can cause systemic inflammatory response syndrome (SIRS) followed by protracted, potentially lethal immunosuppression. The mechanisms responsible for impaired immunity post-SIRS remain unclear. We show that SIRS triggered by pathogen mimics or malaria infection leads to functional paralysis of conventional dendritic cells (cDCs). Paralysis affects several generations of cDCs and impairs immunity for 3–4 weeks. Paralyzed cDCs display distinct transcriptomic and phenotypic signatures and show impaired capacity to capture and present antigens *in vivo*. They also display altered cytokine production patterns upon stimulation. The paralysis program is not initiated in the bone marrow but during final cDC differentiation in peripheral tissues under the influence of local secondary signals that persist after resolution of SIRS. Vaccination with monoclonal antibodies that target cDC receptors or blockade of transforming growth factor β partially overcomes paralysis and immunosuppression. This work provides insights into the mechanisms of paralysis and describes strategies to restore immunocompetence post-SIRS.

## INTRODUCTION

Systemic inflammatory response syndrome (SIRS) is triggered by severe infections (e.g., pneumonia, malaria) or tissue injury (e.g., trauma, major surgery).[1–3] It is characterized by excessive release of inflammatory cytokines that activate innate and adaptive immunity.[4] Paradoxically, SIRS is followed by immunosuppression that can last for weeks, long after clearance of the infection or recovery from injury.[5–7] Patients recovering from SIRS in intensive care units (ICUs) contract opportunistic infections.[8–11] Care of these patients and prevention of infections post-SIRS exert a high-cost burden on the health system.[12] Impaired immunity post-SIRS may also contribute to poor vaccination outcomes and increased susceptibility to secondary infections in malaria-endemic regions.[13,14] Several factors may contribute to immunosuppression post-SIRS. Induction of conventional dendritic cell (cDC) paralysis has been proposed as a major factor,[15] but the underlying mechanisms remain obscure.

cDCs play pivotal roles in innate and adaptive T cell immunity[16,17] owing to their ability to (1) detect pathogens; (2) capture and process exogenous antigen (Ag); (3) (cross-)present Ag via major histocompatibility complex (MHC) class I and/or class II molecules; (4) upregulate costimulatory molecules; (5) secrete cytokines that stimulate natural killer cell and T cell responses; and (6) activate Ag-specific naive T cells. Two subtypes of cDCs have been described, cDC1s and cDC2s, with distinct

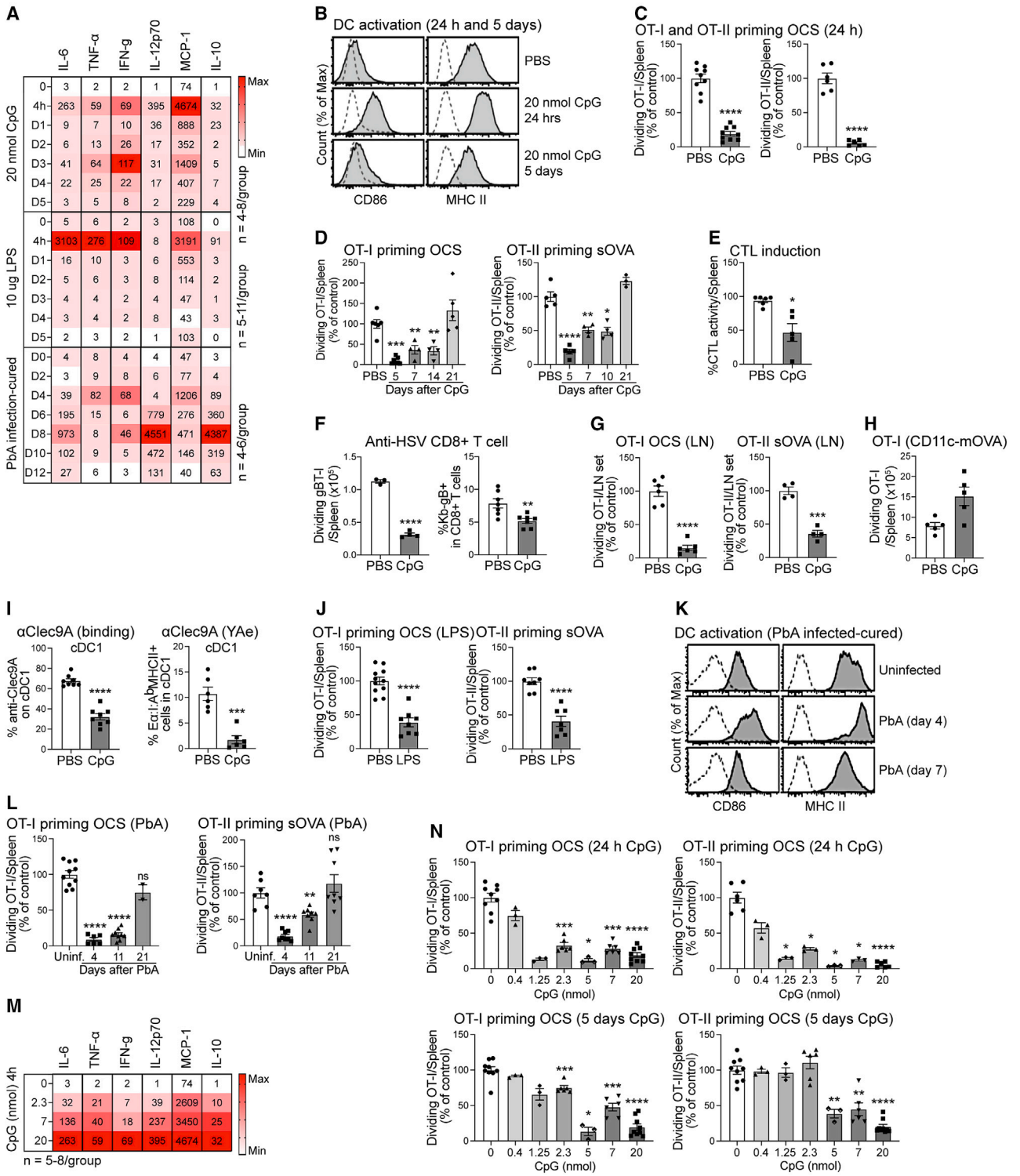


**Figure 1. SIRS induces DC paralysis and protracted immunosuppression in mice**

(A) Concentration of the indicated cytokines in mouse sera at the time points shown following induction of SIRS with intravenous CpG, LPS, or PbA infection-cure.

(B) Expression of activation markers on splenic cDCs 1 and 5 days after CpG injection. Dashed lines: unstained cells.

(C) OT-I and OT-II priming with OCSs in spleen 24 h after CpG injection.

(D) OT-I and OT-II priming with OCSs or sOVA in spleen at the indicated times after CpG injection.

*(legend continued on next page)*

capacities to perform these functions.[18] cDCs have a short half-life and continuously renew in peripheral tissues and secondary lymphoid organs from bone marrow (BM)-derived precursors.[16,19] As the precursors differentiate into cDCs, they are exposed to local cues that affect their acquisition of functional properties, including Ag presentation.[20,21] These cues differ among anatomical locations and can change over time in response to previous infections, implying the functions of cDCs undergo spatiotemporal adaptations (STAs).[22] An extreme form of STA leads to formation of paralyzed cDCs with impaired functions.[15] The functional defects of paralyzed cDCs remain poorly understood, as are the mechanisms that induce paralysis.

Here, we show that SIRS triggered by blood-borne pathogen-associated compounds or malaria infection initiates synchronous paralysis of cDCs in the spleen. We use this approach to characterize the transcriptome and the functional defects of paralyzed cDCs, as well as the site and stage of cDC development at which the paralysis STA is induced. We use this information to devise strategies to overcome cDC paralysis with Ag-targeting monoclonal antibodies (mAbs) and with inhibitors of paralysis-inducing signals. We show these treatments accelerate the restoration of immunocompetence post-SIRS.

## RESULTS

### Blood-borne triggers of SIRS induce DC paralysis and protracted immunosuppression

Intravenous injection of the bacterial mimic CpG into mice induces SIRS,[23,24] with increases in pro- and anti-inflammatory cytokines in serum within 4 h, followed by their gradual decline (Figure 1A). As shown previously,[23,24] SIRS caused systemic cDC activation (Figure 1B), leading to severe impairment of $CD8^+$ (OT-I) and $CD4^+$ (OT-II) T cell priming in the spleen in response to ovalbumin (OVA)-coated splenocytes (OCS) injected 24 h after the induction of SIRS (Figure 1C). This was due to the intrinsic inability of activated cDCs to present newly encountered Ags (Figure S1A).[23] Activated cDCs also displayed altered cytokine secretion patterns in response to CpG encountered post-activation (Figure S1B).

Splenic cDCs have a half-life of less than 3 days.[19] Analysis of BrdU incorporation *in vivo* showed that the rate of replacement of $BrdU^-$ cDCs with $BrdU^+$ cDCs was equivalent in untreated and CpG-treated mice (Figure S1C). Indeed, 5 days after SIRS induction, all the activated splenic cDCs had been replaced by new resting cDCs (Figure 1B).[16,19] Yet, MHC class I or II (cross-)presentation of OVA remained impaired at day 5 and was not fully recovered until day 21 post-CpG treatment (Figure 1D). Induction of anti-OVA cytotoxic T lymphocyte responses from the endogenous repertoire was also impaired after SIRS (Figure 1E), as was cross-priming of CD8 T cells against herpes simplex virus (Figure 1F). T cell priming was impaired in the lymph nodes too (Figure 1G). Defective T cell priming was not due to lack of cDCs in CpG-pretreated mice (Figure S1D). OT-I priming did occur in CpG-pretreated CD11c-mOVA transgenic mice (Figure 1H), in which the cDCs constitutively express and present OVA via the endogenous MHC class I pathway.[23] This indicated that the defect in cross-priming in wild-type (WT) mice post-SIRS was caused by impaired Ag presentation rather than suppression of T cell activation *in vivo*. We tested this hypothesis by measuring Ag presentation with a T cell-independent assay. We injected mice with $\alpha$-Clec9A-IEpep. This protein construct consists of mAb 10B4, specific for the cDC1 receptor Clec9A, fused to a peptide that corresponds to the amino acid sequence 52–68 of mouse $I\text{-}E^b$ (IEpep), presented by the MHC class II molecule $I\text{-}A^b$.[25,26] Capture and, more prominently, presentation of this model Ag by cDC1s was impaired 5 days post-SIRS induction (Figures 1I and S1E). Plasmacytoid DCs and cDC2s express little and no Clec9A, respectively,[27] so binding and presentation of the $\alpha$-Clec9A-IEpep by these cell types were negligible (Figure S1F).

Intravenous injection of lipopolysaccharide (LPS) also caused SIRS, albeit with a different profile of serum cytokines from that elicited by CpG (Figure 1A). Five days after LPS injection (Figure 1J), T cell priming was impaired even though cDC numbers were not reduced (Figure S1G). To determine whether paralysis was also observed following recovery from infection with a live pathogen, we infected mice with the malaria parasite *Plasmodium berghei* ANKA strain (PbA) (Figure S1H). Live blood-stage PbA parasites injected into mice proliferate (Figure S1I), causing SIRS (Figure 1A) and systemic cDC activation (Figure 1K) 4 days after infection,[23] leading to impaired presentation of malaria[28] and other Ags (Figure 1L).[23] PbA-infected mice die of cerebral malaria or anemia if left untreated but can be cured by administering chloroquine on days 4–10 post-infection (Figures S1H and S1I).[29] All the activated splenic cDCs of cured mice had been replaced with resting cDCs on day 7 post-infection (Figure 1K). However, Ag presentation was not recovered until day 21 (Figure 1L). Impaired T cell priming was not due to lack of cDCs (Figure S1J). Therefore, different blood-borne inducers of SIRS cause development of paralyzed cDCs for weeks.

(E–I) Measurement of the following parameters in mice, carried out 5 days after intravenous injection of PBS or CpG: (E) anti-OVA cytotoxic T lymphocyte (CTL) responses induced by OCS+LPS vaccination; (F) anti-HSV gBT-I priming (left) and percentage of $H2\text{-}K^b$gB tetramer-specific $CD8^+$ T cells in spleens (right); (G) OT-I and OT-II priming with OCSs and sOVA, respectively, in lymph nodes (LNs); (H) OT-I priming in spleens of CD11c-mOVA mice; and (I) percentage of splenic cDC1s decorated with anti-Clec9A-$OVA_{FGD}$-A647 (left) and presenting IEpep bound to $I\text{-}A^b$ detected by YAe Ab (right).

(J) OT-I and OT-II priming with OCSs and sOVA, respectively, 5 days after LPS administration.

(K) Expression of activation markers on splenic cDCs of mice infected-cured with PbA. Dashed lines: unstained cells.

(L) OT-I and OT-II priming with OCSs and sOVA, respectively, at the indicated times in PbA infected-cured mice.

(M) Concentration of the indicated cytokines in mice sera 4 h after injection of 0–20 nmol CpG.

(N) OT-I and OT-II priming with OCSs in spleen 24 h (top) or 5 days (bottom) after SIRS induction with the indicated doses of CpG.

PBS refers to injection of vehicle alone (negative control). All results are from at least 2 independent experiments except day 21 in the left (OT-I) graph of (L) (one experiment). Results in (A) and (M) are from 4–11 mice per group. Histograms in (B) and (K) are representative data from more than 4 mice per group. Bar graphs show means ± SEM with each dot corresponding to one mouse. Independent-samples t test. Blank or ns, non-significant; $^*p \leq 0.05$, $^{**}p \leq 0.01$, $^{***}p \leq 0.001$, $^{***}p \leq 0.0001$. See also Figure S1.

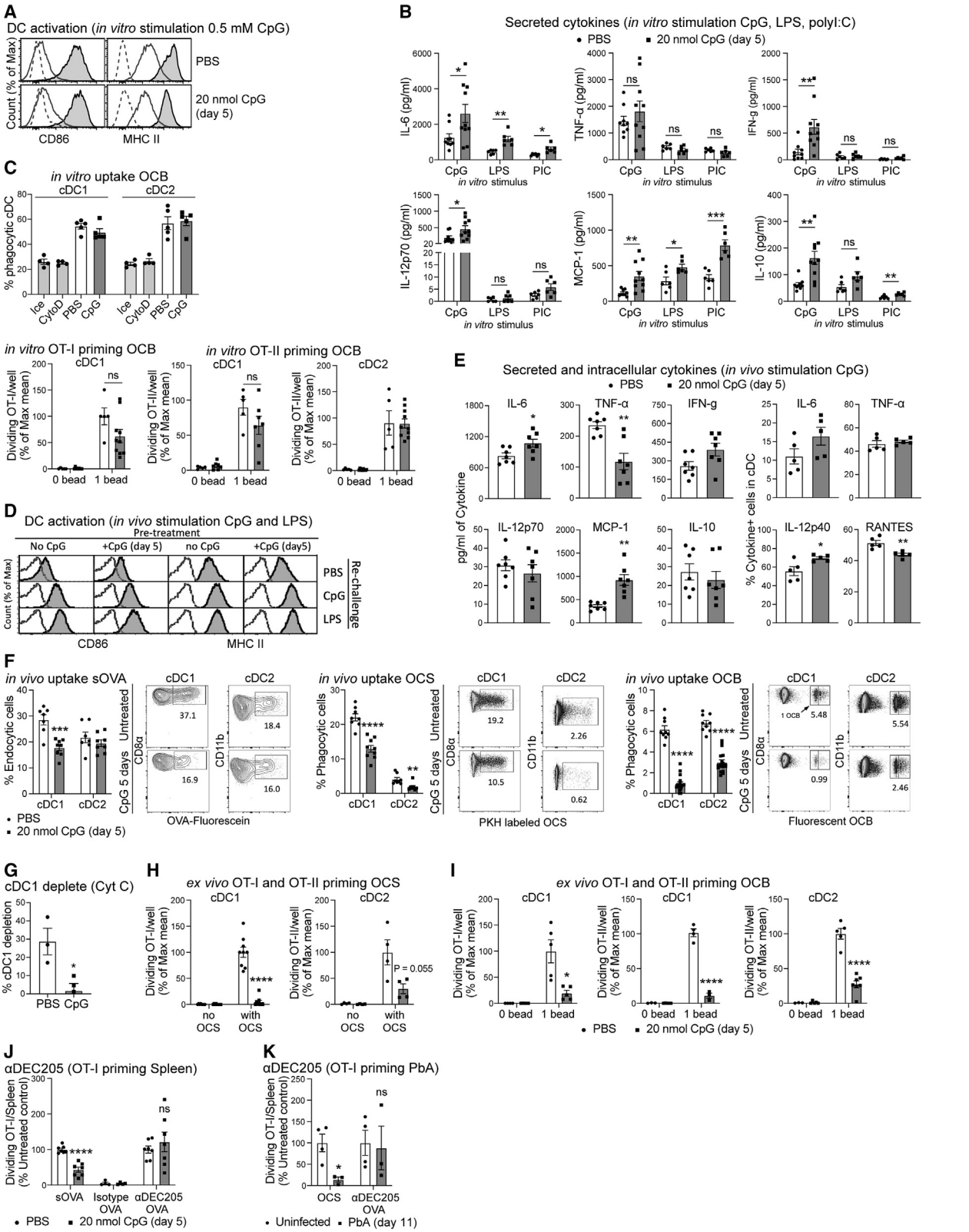


*(legend on next page)*

We have proposed that paralysis is not an automatic consequence of systemic DC activation but an extreme form of STA induced when the inflammatory response reaches a certain threshold.[22] To test this hypothesis, we studied the effect of decreasing doses of CpG on cDC function during and post-SIRS (1 and 5 days after CpG injection, respectively). The severity of SIRS, measured by cytokine concentration in serum, correlated with the CpG dose used (Figure 1M). Impairment of T cell priming *in vivo* during SIRS required $\geq$1.25 nmol CpG, but induction of paralysis post-SIRS required 4 times more CpG ($\geq$5 nmol) (Figure 1N). Thus, the cDCs that replaced those that were systemically activated with a low dose of CpG developed normally, but those that replaced the cDCs activated with a high dose of CpG acquired a paralyzed STA.

## Paralyzed cDCs are functional *in vitro*

Next, we addressed whether the paralysis STA was intrinsically imprinted on the cDCs or maintained by the *in vivo* environment. Paralyzed cDCs purified from the spleens of mice treated 5 days prior with CpG and incubated *in vitro* with CpG upregulated MHC class II and CD86 expression like their counterparts from untreated animals (Figure 2A). They also produced similar or higher levels of cytokines in response to Toll-like receptor (TLR) ligands CpG, LPS, and polyI:C (Figures 2B and S2A). We used fluorescent OVA-coated latex beads (OCBs) to compare *in vitro* the phagocytic capacity of paralyzed cDC1s and cDC2s to that of their normal counterparts and found it to be equivalent (Figure 2C). We purified cells that had phagocytosed one bead (i.e., containing equivalent amounts of OVA) and compared their capacity to prime OT-I and OT-II cells. No significant difference was observed between the cDCs of untreated and CpG-pretreated mice (Figure 2C) (note that cDC2s do not have the ability to cross-present[30]). Presentation of soluble OVA (sOVA) (Figure S2B) and OCSs (Figure S2C) was also comparable. Analysis of paralyzed cDCs from LPS-pretreated mice yielded similar results (Figure S2D). We conclude that paralyzed cDCs retained the capacity to perform the defining properties of cDCs *in vitro*, so they were not intrinsically paralyzed.

## Paralysis of cDCs is maintained *in vivo* but can be overcome by targeting Ag to a receptor

Next, we addressed the functional capabilities of paralyzed cDCs *in vivo*. They upregulated activation markers in response to CpG or LPS injection (Figure 2D), but their cytokine production profiles were altered (Figure 2E). Capture of sOVA by paralyzed cDC2s was normal but partly reduced in cDC1s (Figure 2F), and phagocytosis of OCSs and OCBs was clearly impaired in both cDC subsets (Figures 2F and S2E). Phagocytosis was also impaired in malaria infected-cured mice (Figure S2F). A potential explanation might be that the splenic architecture in mice recovered from SIRS was disrupted, preventing latex beads from reaching cDCs. However, immunohistology analysis did not show overt differences in fluorescent bead signal or localization in the spleens of either set of animals (Figure S2G).

Impairment of OT-I and OT-II priming in mice that recovered from SIRS and were challenged with sOVA (Figure 1D) appeared more profound than the impairment of OVA uptake by their cDCs (Figure 2F), suggesting additional Ag presentation defects post-uptake. Cross-presentation by cDC1s involves the transfer of endocytosed proteins to the cytosol.[31] Due to this activity, ~30% of cDC1s of mice injected with cytochrome *c*, a protein that triggers apoptosis upon its release into the cytosol, die (Figure 2G).[32] Only ~5% of cDC1s of mice treated with CpG 5 days earlier were lost upon cytochrome *c* injection (Figure 2G). This might be partly due to lower capture of soluble proteins by paralyzed cDC1s (Figure 2F) but also suggests paralyzed cDC1s were defective in protein transfer from endosomes to the cytosol.

To characterize further cDC paralysis *in vivo*, we injected fluorescently labeled sOVA, OCSs, or OCBs into untreated and CpG-pretreated mice. We purified cDCs that had captured equivalent amounts of the Ag (e.g., one OCB) or no Ag and incubated them *ex vivo* with OT cells. Paralyzed cDCs were incapable of (cross-)presenting cell- or bead-associated OVA via MHC class I or II (Figures 2H and 2I). They could cross-present via MHC class I, and partially present via MHC class II, sOVA (Figure S2H). From this set of experiments, we conclude that the tissue environment post-SIRS maintains a paralyzed STA in cDCs that impairs Ag (cross-)presentation at a stage downstream of Ag capture.

An efficient way to induce Ag cross-presentation by cDC1s is to target Ags to their surface receptors.[33] We tested if this approach could bypass the paralysis STA and restore T cell priming in mice post-SIRS. CpG-pretreated or PbA infected-cured mice were injected with a construct consisting of OVA

**Figure 2. Functional capabilities of paralyzed cDCs**

(A–C) Mice were injected with CpG, and 5 days later, splenic cDCs were purified and assessed for (A) expression of activation markers after purification (open histograms) or following a 6 h incubation with CpG *in vitro* (shaded) (dashed lines: unstained cells); (B) cytokines secreted *in vitro* after stimulation with CpG, LPS, or poly(I:C), and (C) phagocytosis of fluorescent OCBs on ice or at 37°C in the absence or presence of cytochalasin D.

(D–G) Mice were injected with CpG and the following assessments were performed 5 days later: (D) expression of activation markers by cDCs 24 h after secondary CpG or LPS injection; (E) cytokine production *in vitro* by cDCs purified 2 h after injection of CpG, determined by measuring concentration in supernatant (left) or by intracellular staining (right); (F) capture of intravenously injected sOVA, OCSs, or OCBs; and (G) depletion of splenic cDC1s caused by injection of cytochrome *c*.

(H–I) As in (F), but splenic cDCs that had captured equivalent amounts of OCS (H), one OCB (I), or no Ag in mice that had been injected with PBS (blank bars) or CpG (shaded) were purified and used to prime OT-I or OT-II cells *ex vivo*.

(J) Mice were injected with PBS or CpG. Five days later, the mice were vaccinated with sOVA, anti-DEC205-OVA, or rat IgG2a isotype control, and OT-I priming was measured in the spleen.

(K) OT-I priming in the spleen following vaccination of untreated or PbA infected-cured mice with OCSs or anti-DEC205-OVA.

All results are from at least 2 independent experiments. Histograms in (A) and (D) are representative data from 4–5 mice per group. Bar graphs show means ± SEM with each dot corresponding to one mouse. Independent-samples t test. Blank or ns, non-significant; *p $\leq$ 0.05, **p $\leq$ 0.01, ***p $\leq$ 0.001, ****p $\leq$ 0.0001. See also Figure S2.

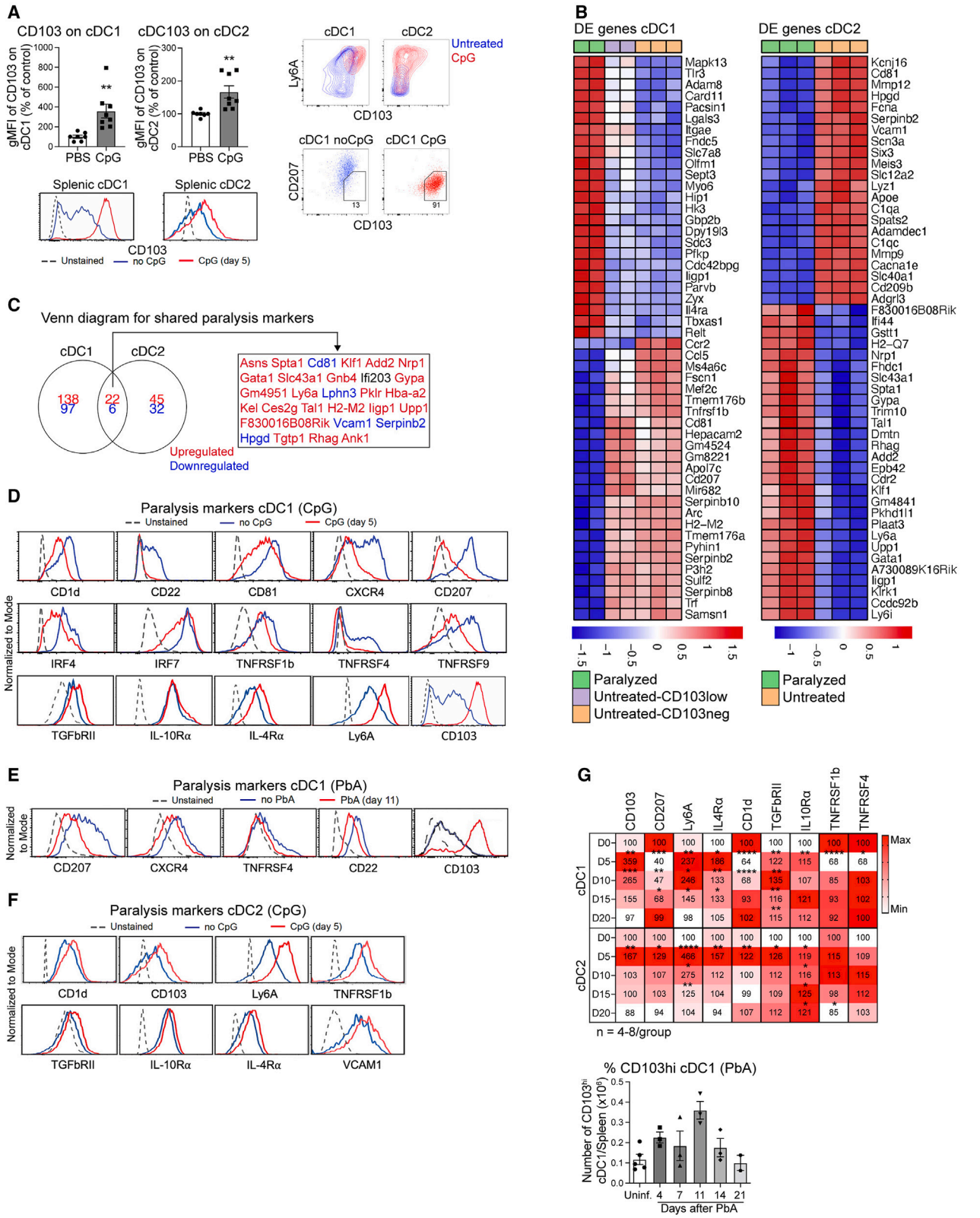


*(legend on next page)*

conjugated to mAb against DEC-205,[34] an endocytic receptor highly expressed on cDC1s,[35] which was similarly expressed by resting and paralyzed cDC1s (Figure S2I). Targeting OVA to this receptor enabled efficient OT-I cross-priming in both CpG-pretreated and PbA infected-cured mice (Figures 2J and 2K).

## SIRS induces a distinct transcriptional program in splenic cDCs

We explored further the hypothesis that the microenvironment post-SIRS induced cDC paralysis. Transforming growth factor β (TGF-β) contributes to formation of paralyzed cDCs in the lung after resolution of severe pneumonia.[15] We reasoned that if it played a similar role in the spleen, it would induce CD103 expression as it does in developing cDC1s *in vitro*.[21] Indeed, splenic cDCs of CpG-pretreated and PbA infected-cured mice showed high CD103 expression, particularly in cDC1s (Figures 3A and 3E). To identify additional hallmarks of cDC paralysis, we compared the transcriptomes of untreated and paralyzed cDC1s and cDC2s. As CD103 is expressed at low levels in a fraction of untreated cDC1s[20] (Figure 3A), we sequenced separately the transcriptomes of $CD103^{neg}$ and $CD103^{low}$ cDC1s to account for the possibility that paralyzed ($CD103^{high}$) and untreated $CD103^{int}$ cDC1s were equivalent. Indeed, these two populations expressed similar transcriptomes except for some genes including *Itgae* (CD103) itself (TREAT false discovery rate > 0.1) (Figure 3B; Table S1). In contrast, 263 genes were differentially expressed in paralyzed cDC1s with fold changes significantly greater than 1.5 compared to the average of the $CD103^{neg}$ and $CD103^{low}$ cDC1 populations (Figures 3B and 3C; Table S1). Expression of the markers that define the cDC1 lineage (*xcr1*, *batf3*, *clec9a*, *dec205*, *btla*, and *cd24*) was conserved in paralyzed cDC1s (ROAST p = 0.001) (Table S1), confirming their cDC1 identity. Comparison of the transcriptomes of untreated and paralyzed cDC2s using the same parameters of significance revealed 105 differentially expressed genes (Figures 3B and 3C; Table S1). At the same time, expression of transcription factors required for cDC2 lineage determination and identity (*irf2*, *irf4*, *klf4*, *notch2*, *itgam*, and *sirpα*) was not different (Table S1). Twenty-nine differentially expressed genes shared by both subsets of paralyzed cDCs defined a common paralysis signature (Figure 3C).

We validated by flow cytometry the differential expression of 13 membrane proteins and 2 transcription factors in paralyzed cDC1s (Figure 3D), which could be defined as $CD103^{high}CD207^{low}Ly6A^{high}$ (Figure 3A). These markers were also differentially expressed in the paralyzed cDC1s of PbA infected-cured mice (Figure 3E). Untreated mice did not contain cDC1s with this phenotype (Figure 3A), confirming that the $CD103^{low}$ cDCs present in these mice were not paralyzed. We also confirmed the differential expression of 8 markers in paralyzed cDC2s (Figure 3F), which could be defined as $CD103^{int}Ly6A^{high}$ (Figure 3A). The kinetics of accumulation and decline of splenic cDCs with the paralyzed phenotype (Figure 3G) correlated with the kinetics of impairment of T cell priming post-SIRS (Figures 1D and 1L). Since the half-life of the splenic cDC compartment is 1.5–3 days,[16,19] but paralysis persisted for 21 days, the paralysis program appeared to affect several generations of cDCs.

## cDCs acquire the paralysis STA during final differentiation *in situ*

To gain insights into the location and stage at which cDCs acquired the paralysis STA, we firstly determined if BM precursors of CpG-treated mice were committed to produce paralyzed cDCs. In Flt3L-supplemented cultures, BM precursors of CpG-treated mice produced cDC1s and cDC2s with similar frequency to their counterparts from untreated mice (Figure S3A). When injected into unpretreated, non-irradiated mice, precursors from the BM of CpG-treated mice produced normal cDCs, but BM precursors of untreated mice produced paralyzed cDCs in mice that had been treated with CpG 5 days earlier (Figures 4A and S3B). Paralysis was therefore induced at a post-BM precursor stage.

BM precursors of cDCs give rise to pre-cDCs, which seed spleen, where they undergo final differentiation into cDCs.[36] The spleens of mice treated 5 days earlier with CpG contained increased numbers of $CD11c^{int}$ cells (Figure 4B) that displayed the phenotype of such precursors (Figure S3C).[36] Indeed, after adoptive transfer to non-irradiated, unpretreated mice, these precursors produced more splenic cDCs on a per-cell basis than fully differentiated cDCs did (Figure 4C). The cDCs generated by $CD11c^{int}$ precursors purified from untreated or CpG-pretreated mice acquired a paralyzed phenotype in CpG-pretreated recipient mice but a normal phenotype in unpretreated recipients (Figures 4D and S3D). This result indicated, first, that SIRS induced "emergency DC-poiesis[37]" that led to increased release of cDC precursors that seeded the spleen and, second, that these precursors were not yet committed to acquire a normal or paralyzed STA, a decision that depended on whether SIRS had occurred in the spleen, where they underwent final differentiation into cDCs. The number of splenic $CD11c^{int}$ precursors peaked at day 5 post-CpG injection but decreased over the next 15 days (Figure 4B), in synchrony with the replacement of

**Figure 3. SIRS induces a distinct transcriptional program in splenic cDCs**

(A) Expression of CD103, Ly6A, and CD207 on splenic cDCs 5 days after CpG treatment.

(B) Heatmap showing relative expression of the top 50 differentially expressed genes (DEGs): (left) among $CD103^{neg}$ and $CD103^{low}$ cDC1s of untreated mice and paralyzed cDC1s of CpG-pretreated mice and (right) between untreated and paralyzed cDC2s.

(C) Number of DEGs (TREAT false discovery rate [FDR] ≤ 0.1, fold changes >1.5) between resting and paralyzed cDC1s and cDC2s. The box lists the DEGs shared by the two cDC subsets.

(D and E) Expression of paralysis markers by cDC1s 5 days after CpG treatment (D) or at day 11 in PbA infected-cured mice (E) and by cDC2s 5 days after CpG treatment (F).

(G) Expression of paralysis markers (top) in cDC1s and cDC2s after SIRS induction with CpG (shown in heatmap are gMFI data normalized to untreated as 100) and (bottom) in cDC1s of PbA infected-cured mice at the indicated times.

All results are from at least 2 independent experiments. Each column in (B) corresponds to an independent cell preparation. Bar graphs show means ± SEM with each dot corresponding to one mouse. Results in (G) (top) are from 4–8 mice per group. Independent-samples t test. Blank, non-significant; *p ≤ 0.05, **p ≤ 0.01, ***p ≤ 0.001, ****p ≤ 0.0001.

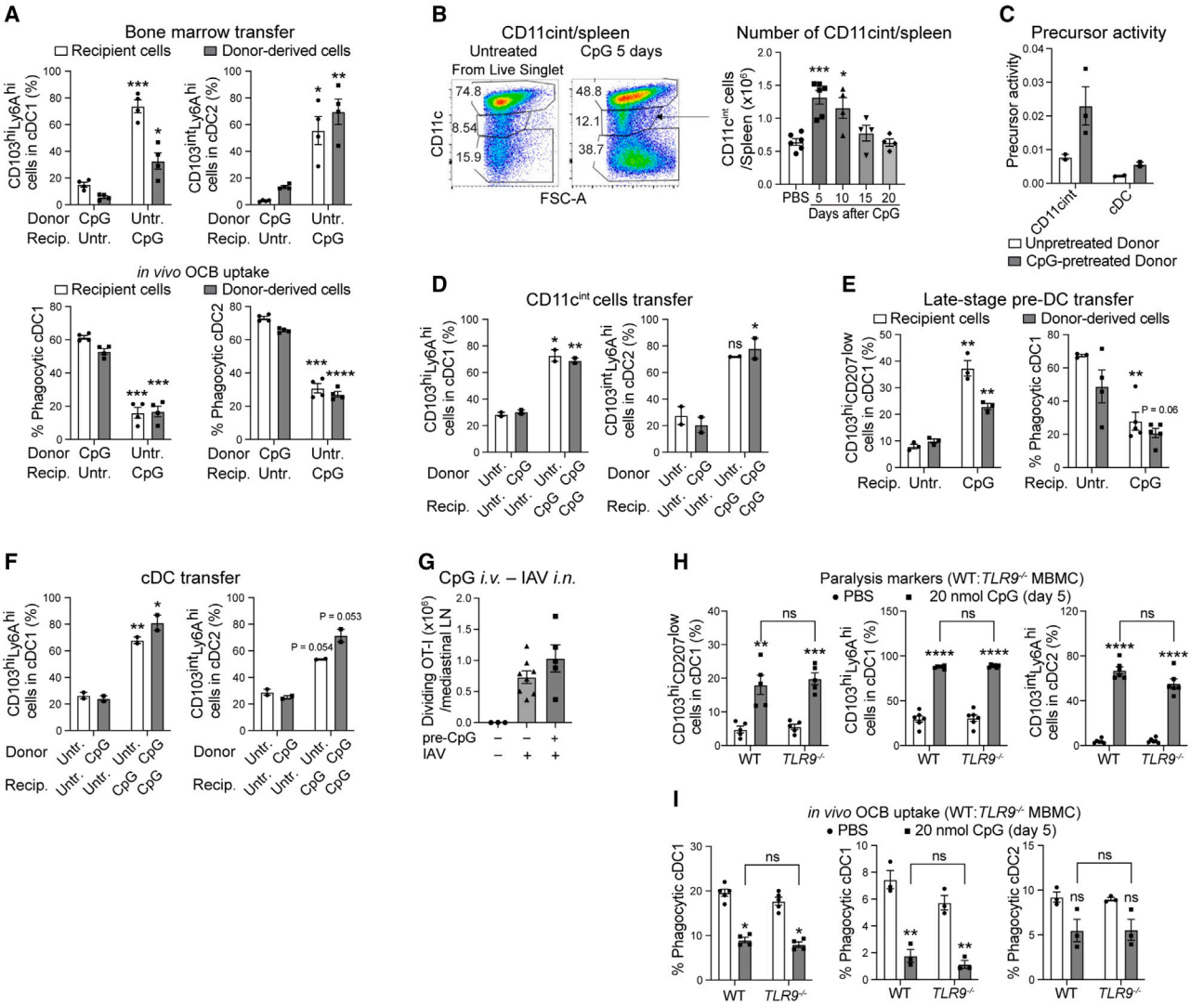


**Figure 4. cDCs acquire the paralysis STA during final differentiation in spleen**

(A) Unpretreated mice were injected with BM cells from CpG-pretreated mice, and CpG-treated mice were injected with BM from untreated mice (Figure S3B). The proportion of paralyzed cDCs derived from the recipient or donor BM cells 3 days after BM injection (top) and their capacity to phagocytose fluorescent OCBs *in vivo* (bottom) are shown.

(B) Number of splenic CD11c$^{int}$ precursors, identified as shown in the representative fluorescence-activated cell sorting (FACS) plots, at the indicated times after CpG injection.

(C) Number of cDCs generated following transfer of CD11c$^{int}$ precursors, or cDCs, purified from untreated or CpG-pretreated mice (Figures S3D and S3F). Shown is the precursor activity on a per-transferred-cell basis.

(D) CD11c$^{int}$ precursors were purified from untreated or CpG-pretreated mice and transferred to mice previously injected with PBS or CpG (Figure S4D). Shown is the proportion of paralyzed cDCs among those derived from the transferred precursors.

(E) As in (D) but after transfer of late-stage pre-cDC1s from untreated, Flt3L-producing tumor-bearing donor mice (Figure S4E). Shown is the proportion of paralyzed cDC1s derived from the recipient's BM or from the transferred precursors (left) and their phagocytic capacity (right).

(F) As in (D) but following transfer of purified cDCs (Figure S4F).

(G) Seven days after intravenous injection of CpG, mice were intranasally infected with x31-OVA, and OT-I priming was measured.

(H and I) Proportion (H) and phagocytic capacity (I) of paralyzed WT or *TLR9*$^{-/-}$ cDCs in mixed BM chimeric mice 5 days after CpG injection. In (I), the left graph shows data for 0.5 μm OCB, and the middle and right graphs show data for 1 μm OCB.

All results are from at least 2 independent experiments except the middle and right graphs in (I) (one experiment each). Bar graphs show means ± SEM with each dot corresponding to one mouse. Independent-samples t test. Blank or ns, non-significant; *p ≤ 0.05, **p ≤ 0.01, ***p ≤ 0.001, ****p ≤ 0.0001.

See also Figure S3.

paralyzed cDCs with normal cDCs (Figure 3G) and the recovery of T cell priming in CpG-pretreated mice (Figure 1D).

The final precursor in cDC1 differentiation increases in quantity in mice bearing Flt3L-producing tumors.[38] Upon transfer into unpretreated or CpG-pretreated recipient mice, these precursors generated cDC1s with a normal or paralyzed phenotype and phagocytic capacity, respectively (Figures 4E and S3E). Finally, fully differentiated cDCs from untreated mice acquired a paralyzed phenotype in CpG-pretreated mice, while paralyzed cDCs became normal after transfer to unpretreated recipients (Figures 4F and S3F). Collectively, these results demonstrate that the paralysis STA is induced late during differentiation in spleen and is reversible. The lack of functional defects in paralyzed cDCs analyzed *in vitro* was consistent with this conclusion.

We have previously shown that airway inflammation causes cDC paralysis in the lungs but not the spleen.[15] Conversely, T cell priming in the lungs against influenza A virus-encoding OVA peptide (SIINFEKL) administered intranasally was unaffected by intravenous pretreatment with CpG (Figure 4G). As cDCs are replaced in all organs from BM-derived precursors, the fact that intravenous CpG induced cDC paralysis in the spleen but not the lungs is consistent with the notion that this STA is imprinted in the affected organ during final cDC differentiation.

It could be argued that paralysis is caused by recognition of small amounts of pathogen-associated compounds persisting at sites of infection or inoculation. To address this possibility, we generated mixed BM chimeric mice where WT recipients received a 1:1 mix of WT and TLR9-deficient BM.[39] TLR9 is an obligatory receptor for CpG, so if residual CpG caused paralysis, then TLR9-deficient cDCs should not become paralyzed in CpG-treated chimeras. However, both WT and TLR9-deficient cDCs acquired the paralyzed phenotype (Figures 4H and S3G) and were impaired at phagocytosis (Figure 4I), confirming this is an STA induced by secondary, endogenous mediators released or maintained by CpG rather than through TLR9 signaling.

### TGF-β blockade reconstitutes immunocompetence post-SIRS

To reveal potential secondary signals that induced the paralyzed STA, we performed ingenuity pathway analysis on the transcriptomic data (Figure 3B; Table S1). This identified IL-10R as a potential regulator of cDC1 and cDC2 paralysis (Figure S4A). However, a pilot experiment blocking IL-10R on days 3–7 or 5–7 after CpG inoculation did not restore OT-I or OT-II cell priming *in vivo*, even though this treatment caused increased levels of IL-10 and inflammatory cytokines in serum (Figures S4B and S4C). We also investigated whether the transcription factor peroxisome proliferator activated receptor γ (Pparγ) mediated cDC paralysis because it was upregulated in the transcriptome of paralyzed cDC1s (Table S1) and because Pparγ induces a hyporesponsive STA in lung macrophages.[40] However, ablation of Pparγ in $CD11c^+$ cells did not prevent cDC paralysis in CpG-treated mice (Figure S4D).

We have shown that TGF-β contributes to inducing cDC paralysis in the lung following bacterial pneumonia.[15] TGF-β recognition causes upregulation of CD103, a marker highly expressed in paralyzed splenic cDC1s, so we tested its role in splenic cDC paralysis. Mice with ablated TGF-β receptor II (TGF-βRII) in $CD11c^+$ cells develop spontaneous autoimmunity at ages older than 12 weeks.[41] To minimize the impact of TGF-βRII deficiency, we generated mixed BM chimeric mice where irradiated WT recipients were reconstituted with two thirds of BM from WT animals and the other one third with BM from either $TGF\beta RII^{fl/fl}$ ($TGF\beta RII^{WT}$) or $TGF\beta R^{fl/fl}/CD11c^{cre}$ ($TGF\beta RII^{cKO}$) mice. The two groups of mice were injected with CpG, which caused comparable SIRS in sera (Figure S4E). After 5, 10, and 15 days, all the cDCs of chimeras where all cells express TGF-βR expressed the paralyzed STA (Figure 5A, S4F, and S4G). In the mice where 1/3 of the cDC did not express TGF-βRII, the TGF-βRII-deficient cDC maintained normal expression of surface markers (Figures 5A, S4F, and S4G), indicating TGF-β recognition is a requirement for the induction of paralysis. Surprisingly though, paralysis was also reduced in the WT cDCs in these chimeras at the three time points measured (Figures 5A, S4F, and S4G). This suggested that when cDCs recognized TGF-β, they themselves contributed to the induction of paralysis. Indeed, expression of TGF-βR and production of latency associated protein[42] were increased in paralyzed cDCs (Figure 5B).

Next, we addressed whether interfering with TGF-β recognition impacted formation of paralyzed cDCs. Injection of anti-TGF-β 1 and 3 days after CpG improved the phagocytosis by cDCs (Figure 5C). Furthermore, cross-priming of OT-I cells and induction of anti-HSV $CD8^+$ T cell responses, activities mediated primarily by cDC,[23] were also enhanced (Figures 5D and 5E). Anti-TGF-β treatment also reduced cDC paralysis in malaria infected-cured mice (Figure 5F).

## DISCUSSION

Our results show that the functional properties of the cDC network following infection can differ from the one that existed before infection, a departure from the classical view where regulatory mechanisms restore homeostasis. Splenic cDCs are continuously replaced by BM-derived precursors.[16,19] These precursors undergo differentiation into resting (formerly known as ''immature'') cDC1s and cDC2s in the spleen itself, acquiring STAs that are partly set by hardwired transcriptional programs and partly by the influence of local factors.[20,21,37] For instance, granulocyte macrophage colony-stimulating factor stimulates the acquisition of cross-presentation capacity in cDC1.[20] In the absence of overt infection, virtually all cDCs remain resting until they die, with a half-life of 1.5–3 days in spleen.[19] These cDCs are highly efficient at capturing and presenting Ags, secreting cytokines, and initiating adaptive immunity. Intravenous injection of TLR ligands activates all splenic cDCs. As activated cDCs no longer capture and present most forms of Ag,[23,24] and stop cytokine secretion,[43] systemic cDC activation impairs immunity against new challenges.[44] The activated cDCs are replaced by new resting cDCs within 5 days. If the activation was induced with a low dose of TLR ligand, the new resting cDCs developed normally. However, higher doses of TLR ligands, or malaria infection, caused SIRS, inducing a local environment where several generations of cDCs acquired a paralyzed STA.

Paralysis was induced by secondary inflammatory signals acting locally at the site of final cDC differentiation, as we have

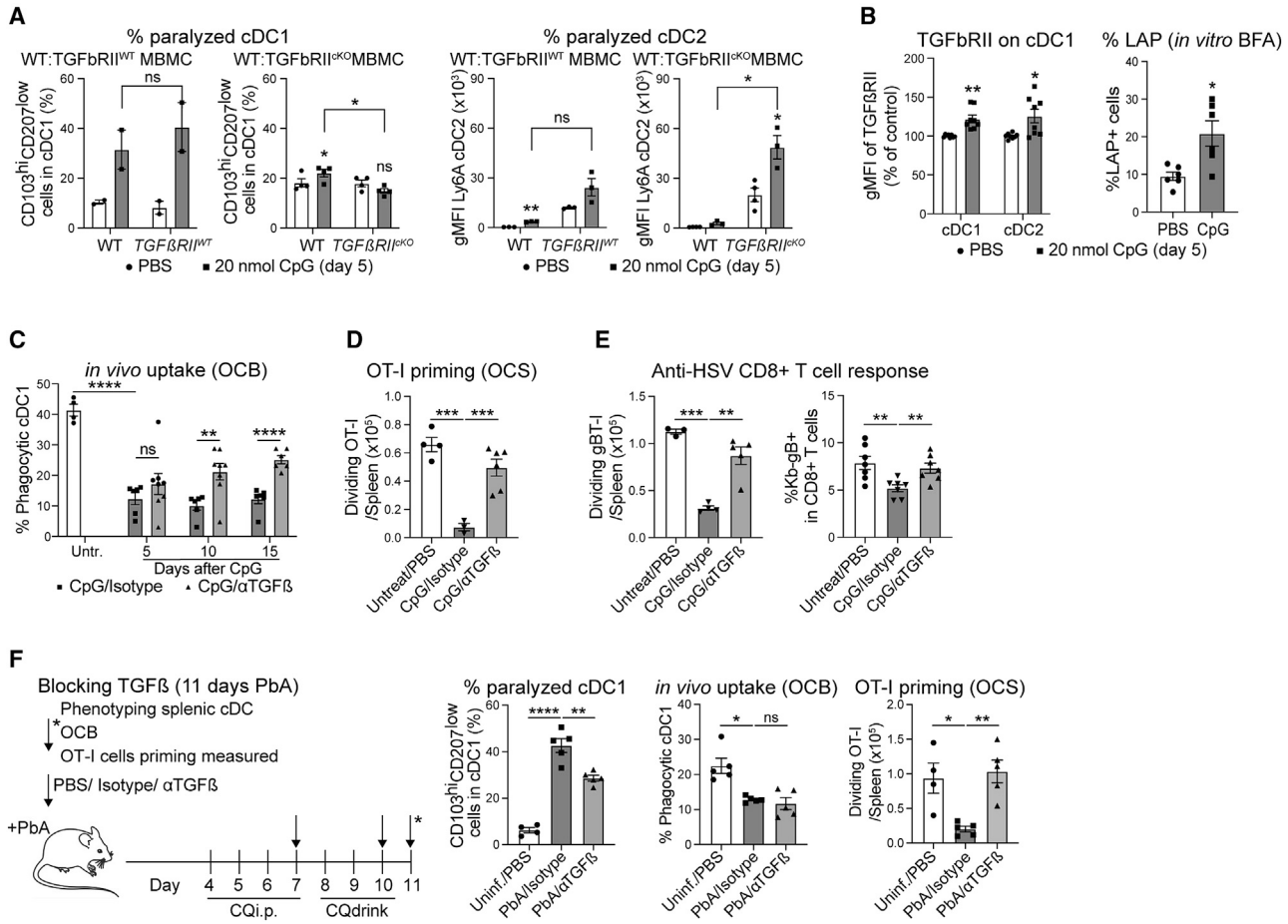


**Figure 5. Role of TGF-β in induction of paralyzed cDCs**

(A) Proportion of paralyzed WT or TGF-βRII-deficient cDCs generated in WT:*TGFβRII*$^{WT}$ or WT:*TGFβRII*$^{cKO}$ mixed BM chimeric mice 5 days after CpG injection.

(B) (Left) Expression of TGF-βRII on splenic cDCs of CpG-treated mice. (Right) Frequencies of latency associated protein (LAP)+ cells after 8 h incubation of splenic cDCs with GolgiPlug 5 days after CpG.

(C–E) Mice were injected with CpG and with anti-TGF-β or isotype control mAb 1 and 3 days after CpG. The following measurements were performed: (C) OCB phagocytosis by splenic cDCs at indicated times after CpG; (D) OT-I priming in response to OCS vaccination 5 days after CpG injection; and (E) gBT-I priming (left) and expansion of H2-K$^b$gB tetramer-specific CD8$^+$ T cells (right) following intravenous HSV infection 5 days after CpG injection.

(F) PbA infected-cured mice were treated with anti-TGF-β or isotype control mAb as shown, and the proportion (left) and phagocytic capacity (middle) of splenic cDC1s and OT-I priming with OCSs (right) were measured on day 11.

All results are from at least 2 independent experiments. Bar graphs show means ± SEM with each dot corresponding to one mouse. Independent-samples t test. ns, non-significant; *p ≤ 0.05, **p ≤ 0.01, ***p ≤ 0.001, ****p ≤ 0.0001.

See also Figure S4.

shown previously that lung inflammation does not induce splenic cDC paralysis,[15] and here we showed that intravenous CpG injection did not affect lung cDC function. More severe SIRS may cause more widespread cDC paralysis, a situation that is probably more common in patients in the ICU in whom SIRS causes organ damage.[11] In such situations, induction of the paralysis STA may commence in BM precursors,[45] but we showed here that local *in situ* factors are sufficient to induce the paralysis STA even on cDCs derived from BM precursors of animals that were not exposed to any inflammatory stimulus at all. Conversely, cDC precursors of mice that suffered SIRS developed normally in healthy recipient animals. This observation also implies that induction of paralyzed cDCs lasts for as long as the signals that induce the paralysis STA persist in the affected organ. In the experimental models analyzed here, it took ~21 days to observe full recovery, implying that at least four generations of newly formed splenic cDCs underwent paralysis. We hypothesized that blockade of paralysis-inducing factors may hasten recovery. Indeed, blocking TGF-β induced formation of immunocompetent cDCs post-SIRS, although it is likely that other factors may also be involved. These may include other cytokines, surface receptors, stromal components, the metabolic status of the tissue, and microbial products. Identification of these factors, the cells that produce them, and the mechanisms responsible for their formation and persistence is an important subject for future studies.[22]

Understanding how the paralysis STA changes the phenotype and function of cDCs is as important as the description of the factors that promote it. Normal and paralyzed cDCs differed in the expression of several surface markers, enabling quantitation of their formation over time following SIRS. We have shown that at least some of the phenotypic changes that characterize human paralyzed cDCs or macrophages can be detected in circulating cells,[11] illustrating the diagnostic value of these findings. The ability to predict which patients with SIRS may be more susceptible to secondary infections may improve their management, reduce the costs associated with their care, and reduce the use of antibiotics, in turn helping to impair the emergence of antibiotic-resistant pathogens.[12]

With regard to functional defects, we have identified that Ag uptake, and in particular phagocytosis, is severely impaired in paralyzed cDCs. We also observed impaired presentation of the (reduced) amount of Ag that was phagocytosed by the paralyzed cDCs. MHC class I and II molecules were expressed on the surface of normal and paralyzed cDCs at equivalent levels. Since MHC molecules are only expressed on the cell surface if they are bound to self or foreign peptide Ags, the defect in presentation of endocytosed Ag cannot be attributed to overt defects in MHC expression, peptide production, or assembly and transport of MHC-peptide complexes. Rather, we propose that some of the steps required for peptides derived from captured Ags to intersect the MHC class I and II (cross-)presentation pathways are impaired in paralyzed cDCs. Protein transfer to the cytosol, required for cross-presentation, was one. This conclusion aligns with the concept, supported by other studies, showing that the efficiency of presentation of endocytosed Ag is influenced by the specific mechanism of capture or the fate of the endosomal compartments containing Ag.[33,46,47] Interestingly, we showed here that these regulatory mechanisms are under the influence of the tissue environment because cDCs that were impaired in presentation of Ag captured *in vivo* were able to capture and present Ag *in vitro*. Furthermore, we were able to partially overcome the Ag cross-presentation defects of cDC1s *in vivo* by targeting the Ag to a surface receptor, showcasing how the characterization of functional defects can lead to restorative strategies potentially applicable to the clinic.

In summary, the findings presented here contribute to understanding the basis for the paradoxical immunosuppression that follows recovery from SIRS and why the duration exceeds the lifespan of cDCs. They also provide a potential explanation for the reduced effectiveness of vaccines in malaria-endemic areas, where individuals may suffer frequent episodes of mild to severe systemic inflammation that may prevent effective uptake and presentation of vaccines against malaria and other pathogens.[14] In such individuals, cDCs may undergo an STA that sets the threshold of responsiveness to a higher, less effective level than in individuals exposed to lower pathogen burdens. Measuring the expression levels of immunocompetence markers on cDCs, delaying the time of vaccination until cDC paralysis wanes, or designing vaccines to target more effectively MHC presentation pathways are potential strategies to overcome immune paralysis.

### Limitations of the study

Only one experiment, using the indicated number of mice, was performed to obtain the following data points: day 21 in the left graph of Figure 1L (n = 2), the middle and right graphs of Figure 4I (n = 3), the top left graph of Figure S2B (n = 3), and the top graphs in Figures S4B (n = 3), S4C (n = 3), and S4F (n = 2).

## STAR★METHODS

Detailed methods are provided in the online version of this paper and include the following:

- KEY RESOURCES TABLE
- RESOURCE AVAILABILITY
  - Lead contact
  - Materials availability
  - Data and code availability
- EXPERIMENTAL MODEL AND STUDY PARTICIPANT DETAILS
  - Mice
- METHOD DETAILS
  - Induction of systemic inflammatory response syndrome
  - Induction and monitoring of blood stage malaria infection
  - Cytokine profiling in sera and culture supernatants
  - Preparation of CellTrace violet-labeled T-cells
  - Preparation of cell-associated OVA
  - Preparation of fluorescent OVA-coated beads (OCB)
  - Priming of OT-cells *in vivo*
  - *In vivo* CTL assay
  - Presentation of viral antigens after CpG
  - BrdU incorporation
  - Preparation of single cells from spleen
  - cDC isolation, analysis and culture
  - RNA-seq expression profiling
  - Cytochrome C-induced depletion of cross-presenting cDC1
  - *In vitro* phagocytosis assays
  - *In vivo* endocytosis and phagocytosis assays
  - Intracellular staining of cytokines
  - *ex vivo* priming of OT-cells
  - Spleen confocal fluorescence microscopy
  - Generation of full or mixed bone marrow chimeras
  - Enrichment of CD11cint cells
  - Late stage pre-DC cells
  - Cell transfer to non-irradiated mice
  - Induction of influenza A virus pulmonary infection
  - PCR for genotyping *Itgax*-Cre and *PPARγ*$^{fl/fl}$ mice
  - Antibodies used for targeting and blocking
- QUANTIFICATION AND STATISTICAL ANALYSIS

## SUPPLEMENTAL INFORMATION

Supplemental information can be found online at https://doi.org/10.1016/j.celrep.2024.113754.

## ACKNOWLEDGMENTS

This work was supported by the National Health and Medical Research Council of Australia (NHMRC) Fellowships 1154970 (G.K.S.), 1058193 (J.A.V.), and 1154502 (J.A.V.), program grants 1016629 (W.R.H., K.S., and J.A.V.) and

1113293 (W.R.H. and J.A.V.), and project grant 1163090 (A.R. and J.A.V.); the Société Française d'Anesthésie et de Réanimation (A.R.); the Fondation des Gueules Cassées (A.R.); Agence National pour le Recherche (A.R.); and the Fundacion Pedro i Pons (J.V.-R.). We thank Prof Axel Kallies (University of Melbourne) for the TGFβR-II$^{fl/fl}$ CD11c$^{cre}$ mice.

## AUTHOR CONTRIBUTIONS

Conceptualization, J.A.V., M.A., J.V.-R., and A.R.; data curation, M.A., J.V.-R., A.R., D.F.-R., S.V., A.T.L.L., J.T.W, L.J.Y., and A.Y.; formal analysis, M.A., J.V.-R., A.R., A.T.L.L., and A.Y.; funding acquisition, J.A.V., A.R., G.K.S., and W.R.H.; investigation, M.A., J.V.-R., and A.R.; methodology, M.A., J.V.-R., and A.R.; resources, J.A.V., Y.Z., L.W., I.C., M.H.L., A.M.L., K.S., W.R.H., and J.D.M.; software, G.K.S. and A.T.L.L.; supervision, J.A.V.; validation, J.A.V.; visualization, M.A.; writing – original draft, M.A., J.V.-R., and J.A.V.; writing – review and editing, M.A., A.R., and J.A.V.

## DECLARATION OF INTERESTS

M.H.L., I.C., and K.S. are listed as inventors on patents relating to Clec9A antibodies.

Received: July 4, 2023
Revised: December 1, 2023
Accepted: January 22, 2024
Published: February 13, 2024

## REFERENCES

1. Singer, M., Deutschman, C.S., Seymour, C.W., Shankar-Hari, M., Annane, D., Bauer, M., Bellomo, R., Bernard, G.R., Chiche, J.D., Coopersmith, C.M., et al. (2016). The Third International Consensus Definitions for Sepsis and Septic Shock (Sepsis-3). JAMA *315*, 801–810. https://doi.org/10.1001/jama.2016.0287.
2. Huang, C., Wang, Y., Li, X., Ren, L., Zhao, J., Hu, Y., Zhang, L., Fan, G., Xu, J., Gu, X., et al. (2020). Clinical features of patients infected with 2019 novel coronavirus in Wuhan, China. Lancet *395*, 497–506. https://doi.org/10.1016/S0140-6736(20)30183-5.
3. Fried, M., Kurtis, J.D., Swihart, B., Pond-Tor, S., Barry, A., Sidibe, Y., Gaoussou, S., Traore, M., Keita, S., Mahamar, A., et al. (2017). Systemic Inflammatory Response to Malaria During Pregnancy Is Associated With Pregnancy Loss and Preterm Delivery. Clin. Infect. Dis. *65*, 1729–1735. https://doi.org/10.1093/cid/cix623.
4. Bosmann, M., and Ward, P.A. (2013). The inflammatory response in sepsis. Trends Immunol. *34*, 129–136. https://doi.org/10.1016/j.it.2012.09.004.
5. Adib-Conquy, M., and Cavaillon, J.M. (2009). Compensatory anti-inflammatory response syndrome. Thromb. Haemostasis *101*, 36–47.
6. Hotchkiss, R.S., Monneret, G., and Payen, D. (2013). Sepsis-induced immunosuppression: from cellular dysfunctions to immunotherapy. Nat. Rev. Immunol. *13*, 862–874. https://doi.org/10.1038/nri3552.
7. Roquilly, A., and Villadangos, J.A. (2015). The role of dendritic cell alterations in susceptibility to hospital-acquired infections during critical-illness related immunosuppression. Mol. Immunol. *68*, 120–123. https://doi.org/10.1016/j.molimm.2015.06.030.
8. Walton, A.H., Muenzer, J.T., Rasche, D., Boomer, J.S., Sato, B., Brownstein, B.H., Pachot, A., Brooks, T.L., Deych, E., Shannon, W.D., et al. (2014). Reactivation of multiple viruses in patients with sepsis. PLoS One *9*, e98819. https://doi.org/10.1371/journal.pone.0098819.
9. Vincent, J.L., Sakr, Y., Singer, M., Martin-Loeches, I., Machado, F.R., Marshall, J.C., Finfer, S., Pelosi, P., Brazzi, L., Aditianingsih, D., et al. (2020). Prevalence and Outcomes of Infection Among Patients in Intensive Care Units in 2017. JAMA *323*, 1478–1487. https://doi.org/10.1001/jama.2020.2717.
10. Zhou, F., Yu, T., Du, R., Fan, G., Liu, Y., Liu, Z., Xiang, J., Wang, Y., Song, B., Gu, X., et al. (2020). Clinical course and risk factors for mortality of adult inpatients with COVID-19 in Wuhan, China: a retrospective cohort study. Lancet *395*, 1054–1062. https://doi.org/10.1016/S0140-6736(20)30566-3.
11. Chaumette, T., Cinotti, R., Mollé, A., Solomon, P., Castain, L., Fourgeux, C., McWilliam, H.E.G., Misme-Aucouturier, B., Broquet, A., Jacqueline, C., et al. (2022). Monocyte Signature Associated with Herpes Simplex Virus Reactivation and Neurological Recovery after Brain Injury. Am. J. Respir. Crit. Care Med. *206*, 295–310. https://doi.org/10.1164/rccm.202110-2324OC.
12. Roquilly, A., Torres, A., Villadangos, J.A., Netea, M.G., Dickson, R., Becher, B., and Asehnoune, K. (2019). Pathophysiological role of respiratory dysbiosis in hospital-acquired pneumonia. Lancet Respir. Med. *7*, 710–720. https://doi.org/10.1016/S2213-2600(19)30140-7.
13. Moormann, A.M., Snider, C.J., and Chelimo, K. (2011). The company malaria keeps: how co-infection with Epstein-Barr virus leads to endemic Burkitt lymphoma. Curr. Opin. Infect. Dis. *24*, 435–441. https://doi.org/10.1097/QCO.0b013e328349ac4f.
14. Nunes-Cabaço, H., Moita, D., and Prudêncio, M. (2022). Five decades of clinical assessment of whole-sporozoite malaria vaccines. Front. Immunol. *13*, 977472. https://doi.org/10.3389/fimmu.2022.977472.
15. Roquilly, A., McWilliam, H.E.G., Jacqueline, C., Tian, Z., Cinotti, R., Rimbert, M., Wakim, L., Caminschi, I., Lahoud, M.H., Belz, G.T., et al. (2017). Local Modulation of Antigen-Presenting Cell Development after Resolution of Pneumonia Induces Long-Term Susceptibility to Secondary Infections. Immunity *47*, 135–147.e5, e135. https://doi.org/10.1016/j.immuni.2017.06.021.
16. Merad, M., Sathe, P., Helft, J., Miller, J., and Mortha, A. (2013). The dendritic cell lineage: ontogeny and function of dendritic cells and their subsets in the steady state and the inflamed setting. Annu. Rev. Immunol. *31*, 563–604. https://doi.org/10.1146/annurev-immunol-020711-074950.
17. Curtsinger, J.M., and Mescher, M.F. (2010). Inflammatory cytokines as a third signal for T cell activation. Curr. Opin. Immunol. *22*, 333–340. https://doi.org/10.1016/j.coi.2010.02.013.
18. Villadangos, J.A., and Schnorrer, P. (2007). Intrinsic and cooperative antigen-presenting functions of dendritic-cell subsets in vivo. Nat. Rev. Immunol. *7*, 543–555. https://doi.org/10.1038/nri2103.
19. Kamath, A.T., Pooley, J., O'Keeffe, M.A., Vremec, D., Zhan, Y., Lew, A.M., D'Amico, A., Wu, L., Tough, D.F., and Shortman, K. (2000). The development, maturation, and turnover rate of mouse spleen dendritic cell populations. J. Immunol. *165*, 6762–6770. https://doi.org/10.4049/jimmunol.165.12.6762.
20. Zhan, Y., Carrington, E.M., van Nieuwenhuijze, A., Bedoui, S., Seah, S., Xu, Y., Wang, N., Mintern, J.D., Villadangos, J.A., Wicks, I.P., and Lew, A.M. (2011). GM-CSF increases cross-presentation and CD103 expression by mouse CD8$^+$ spleen dendritic cells. Eur. J. Immunol. *41*, 2585–2595. https://doi.org/10.1002/eji.201141540.
21. Sathe, P., Pooley, J., Vremec, D., Mintern, J., Jin, J.O., Wu, L., Kwak, J.Y., Villadangos, J.A., and Shortman, K. (2011). The acquisition of antigen cross-presentation function by newly formed dendritic cells. J. Immunol. *186*, 5184–5192. https://doi.org/10.4049/jimmunol.1002683.
22. Roquilly, A., Mintern, J.D., and Villadangos, J.A. (2022). Spatiotemporal Adaptations of Macrophage and Dendritic Cell Development and Function. Annu. Rev. Immunol. *40*, 525–557. https://doi.org/10.1146/annurev-immunol-101320-031931.
23. Wilson, N.S., Behrens, G.M.N., Lundie, R.J., Smith, C.M., Waithman, J., Young, L., Forehan, S.P., Mount, A., Steptoe, R.J., Shortman, K.D., et al. (2006). Systemic activation of dendritic cells by Toll-like receptor ligands or malaria infection impairs cross-presentation and antiviral immunity. Nat. Immunol. *7*, 165–172. https://doi.org/10.1038/ni1300.
24. Young, L.J., Wilson, N.S., Schnorrer, P., Mount, A., Lundie, R.J., La Gruta, N.L., Crabb, B.S., Belz, G.T., Heath, W.R., and Villadangos, J.A. (2007). Dendritic cell preactivation impairs MHC class II presentation of vaccines

and endogenous viral antigens. Proc. Natl. Acad. Sci. USA *104*, 17753–17758. https://doi.org/10.1073/pnas.0708622104.

25. Rudensky, A., Rath, S., Preston-Hurlburt, P., Murphy, D.B., and Janeway, C.A., Jr. (1991). On the complexity of self. Nature *353*, 660–662. https://doi.org/10.1038/353660a0.
26. Schriek, P., Ching, A.C., Moily, N.S., Moffat, J., Beattie, L., Steiner, T.M., Hosking, L.M., Thurman, J.M., Holers, V.M., Ishido, S., et al. (2022). Marginal zone B cells acquire dendritic cell functions by trogocytosis. Science *375*, eabf7470. https://doi.org/10.1126/science.abf7470.
27. Caminschi, I., Proietto, A.I., Ahmet, F., Kitsoulis, S., Shin Teh, J., Lo, J.C.Y., Rizzitelli, A., Wu, L., Vremec, D., van Dommelen, S.L.H., et al. (2008). The dendritic cell subtype-restricted C-type lectin Clec9A is a target for vaccine enhancement. Blood *112*, 3264–3273. https://doi.org/10.1182/blood-2008-05-155176.
28. Lundie, R.J., Young, L.J., Davey, G.M., Villadangos, J.A., Carbone, F.R., Heath, W.R., and Crabb, B.S. (2010). Blood-stage Plasmodium berghei infection leads to short-lived parasite-associated antigen presentation by dendritic cells. Eur. J. Immunol. *40*, 1674–1681. https://doi.org/10.1002/eji.200939265.
29. Lau, L.S., Fernandez-Ruiz, D., Mollard, V., Sturm, A., Neller, M.A., Cozijnsen, A., Gregory, J.L., Davey, G.M., Jones, C.M., Lin, Y.H., et al. (2014). CD8+ T cells from a novel T cell receptor transgenic mouse induce liver-stage immunity that can be boosted by blood-stage infection in rodent malaria. PLoS Pathog. *10*, e1004135. https://doi.org/10.1371/journal.ppat.1004135.
30. Schnorrer, P., Behrens, G.M.N., Wilson, N.S., Pooley, J.L., Smith, C.M., El-Sukkari, D., Davey, G., Kupresanin, F., Li, M., Maraskovsky, E., et al. (2006). The dominant role of CD8+ dendritic cells in cross-presentation is not dictated by antigen capture. Proc. Natl. Acad. Sci. USA *103*, 10729–10734. https://doi.org/10.1073/pnas.0601956103.
31. Segura, E., and Villadangos, J.A. (2011). A modular and combinatorial view of the antigen cross-presentation pathway in dendritic cells. Traffic *12*, 1677–1685. https://doi.org/10.1111/j.1600-0854.2011.01254.x.
32. Lin, M.L., Zhan, Y., Proietto, A.I., Prato, S., Wu, L., Heath, W.R., Villadangos, J.A., and Lew, A.M. (2008). Selective suicide of cross-presenting CD8+ dendritic cells by cytochrome c injection shows functional heterogeneity within this subset. Proc. Natl. Acad. Sci. USA *105*, 3029–3034. https://doi.org/10.1073/pnas.0712394105.
33. Reuter, A., Panozza, S.E., Macri, C., Dumont, C., Li, J., Liu, H., Segura, E., Vega-Ramos, J., Gupta, N., Caminschi, I., et al. (2015). Criteria for dendritic cell receptor selection for efficient antibody-targeted vaccination. J. Immunol. *194*, 2696–2705. https://doi.org/10.4049/jimmunol.1402535.
34. Lahoud, M.H., Ahmet, F., Kitsoulis, S., Wan, S.S., Vremec, D., Lee, C.N., Phipson, B., Shi, W., Smyth, G.K., Lew, A.M., et al. (2011). Targeting antigen to mouse dendritic cells via Clec9A induces potent CD4 T cell responses biased toward a follicular helper phenotype. J. Immunol. *187*, 842–850. https://doi.org/10.4049/jimmunol.1101176.
35. Wakim, L.M., Smith, J., Caminschi, I., Lahoud, M.H., and Villadangos, J.A. (2015). Antibody-targeted vaccination to lung dendritic cells generates tissue-resident memory CD8 T cells that are highly protective against influenza virus infection. Mucosal Immunol. *8*, 1060–1071. https://doi.org/10.1038/mi.2014.133.
36. Naik, S.H., Metcalf, D., van Nieuwenhuijze, A., Wicks, I., Wu, L., O'Keeffe, M., and Shortman, K. (2006). Intrasplenic steady-state dendritic cell precursors that are distinct from monocytes. Nat. Immunol. *7*, 663–671. https://doi.org/10.1038/ni1340.
37. Cabeza-Cabrerizo, M., van Blijswijk, J., Wienert, S., Heim, D., Jenkins, R.P., Chakravarty, P., Rogers, N., Frederico, B., Acton, S., Beerling, E., et al. (2019). Tissue clonality of dendritic cell subsets and emergency DCpoiesis revealed by multicolor fate mapping of DC progenitors. Sci. Immunol. *4*, eaaw1941. https://doi.org/10.1126/sciimmunol.aaw1941.
38. Bedoui, S., Prato, S., Mintern, J., Gebhardt, T., Zhan, Y., Lew, A.M., Heath, W.R., Villadangos, J.A., and Segura, E. (2009). Characterization of an immediate splenic precursor of CD8+ dendritic cells capable of inducing antiviral T cell responses. J. Immunol. *182*, 4200–4207. https://doi.org/10.4049/jimmunol.0802286.
39. Vega-Ramos, J., Roquilly, A., Zhan, Y., Young, L.J., Mintern, J.D., and Villadangos, J.A. (2014). Inflammation conditions mature dendritic cells to retain the capacity to present new antigens but with altered cytokine secretion function. J. Immunol. *193*, 3851–3859. https://doi.org/10.4049/jimmunol.1303215.
40. Reddy, R.C., Keshamouni, V.G., Jaigirdar, S.H., Zeng, X., Leff, T., Thannickal, V.J., and Standiford, T.J. (2004). Deactivation of murine alveolar macrophages by peroxisome proliferator-activated receptor-gamma ligands. Am. J. Physiol. Lung Cell Mol. Physiol. *286*, L613–L619. https://doi.org/10.1152/ajplung.00206.2003.
41. Ramalingam, R., Larmonier, C.B., Thurston, R.D., Midura-Kiela, M.T., Zheng, S.G., Ghishan, F.K., and Kiela, P.R. (2012). Dendritic cell-specific disruption of TGF-beta receptor II leads to altered regulatory T cell phenotype and spontaneous multiorgan autoimmunity. J. Immunol. *189*, 3878–3893. https://doi.org/10.4049/jimmunol.1201029.
42. Travis, M.A., and Sheppard, D. (2014). TGF-beta activation and function in immunity. Annu. Rev. Immunol. *32*, 51–82. https://doi.org/10.1146/annurev-immunol-032713-120257.
43. Reis e Sousa, C., Yap, G., Schulz, O., Rogers, N., Schito, M., Aliberti, J., Hieny, S., and Sher, A. (1999). Paralysis of dendritic cell IL-12 production by microbial products prevents infection-induced immunopathology. Immunity *11*, 637–647. https://doi.org/10.1016/s1074-7613(00)80138-7.
44. Vega-Ramos, J., Roquilly, A., Asehnoune, K., and Villadangos, J.A. (2014). Modulation of dendritic cell antigen presentation by pathogens, tissue damage and secondary inflammatory signals. Curr. Opin. Pharmacol. *17*, 64–70. https://doi.org/10.1016/j.coph.2014.07.013.
45. Pastille, E., Didovic, S., Brauckmann, D., Rani, M., Agrawal, H., Schade, F.U., Zhang, Y., and Flohé, S.B. (2011). Modulation of dendritic cell differentiation in the bone marrow mediates sustained immunosuppression after polymicrobial sepsis. J. Immunol. *186*, 977–986. https://doi.org/10.4049/jimmunol.1001147.
46. Alloatti, A., Kotsias, F., Magalhaes, J.G., and Amigorena, S. (2016). Dendritic cell maturation and cross-presentation: timing matters. Immunol. Rev. *272*, 97–108. https://doi.org/10.1111/imr.12432.
47. Blander, J.M. (2018). Regulation of the Cell Biology of Antigen Cross-Presentation. Annu. Rev. Immunol. *36*, 717–753. https://doi.org/10.1146/annurev-immunol-041015-055523.
48. Jenkins, M.R., Webby, R., Doherty, P.C., and Turner, S.J. (2006). Addition of a prominent epitope affects influenza A virus-specific CD8+ T cell immunodominance hierarchies when antigen is limiting. J. Immunol. *177*, 2917–2925. https://doi.org/10.4049/jimmunol.177.5.2917.
49. Segura, E., Kapp, E., Gupta, N., Wong, J., Lim, J., Ji, H., Heath, W.R., Simpson, R., and Villadangos, J.A. (2010). Differential expression of pathogen-recognition molecules between dendritic cell subsets revealed by plasma membrane proteomic analysis. Mol. Immunol. *47*, 1765–1773. https://doi.org/10.1016/j.molimm.2010.02.028.
50. Nikolić-Zugić, J., and Carbone, F.R. (1990). The effect of mutations in the MHC class I peptide binding groove on the cytotoxic T lymphocyte recognition of the Kb-restricted ovalbumin determinant. Eur. J. Immunol. *20*, 2431–2437. https://doi.org/10.1002/eji.1830201111.
51. Hogquist, K.A., Jameson, S.C., Heath, W.R., Howard, J.L., Bevan, M.J., and Carbone, F.R. (1994). T cell receptor antagonist peptides induce positive selection. Cell *76*, 17–27. https://doi.org/10.1016/0092-8674(94)90169-4.
52. Barnden, M.J., Allison, J., Heath, W.R., and Carbone, F.R. (1998). Defective TCR expression in transgenic mice constructed using cDNA-based alpha- and beta-chain genes under the control of heterologous regulatory elements. Immunol. Cell Biol. *76*, 34–40. https://doi.org/10.1046/j.1440-1711.1998.00709.x.
53. Mueller, S.N., Heath, W., McLain, J.D., Carbone, F.R., and Jones, C.M. (2002). Characterization of two TCR transgenic mouse lines specific for

herpes simplex virus. Immunol. Cell Biol. *80*, 156–163. https://doi.org/10.1046/j.1440-1711.2002.01071.x.

54. Prato, S., Zhan, Y., Mintern, J.D., and Villadangos, J.A. (2013). Rapid deletion and inactivation of CTLs upon recognition of a number of target cells over a critical threshold. J. Immunol. *191*, 3534–3544. https://doi.org/10.4049/jimmunol.1300803.
55. Bedoui, S., Whitney, P.G., Waithman, J., Eidsmo, L., Wakim, L., Caminschi, I., Allan, R.S., Wojtasiak, M., Shortman, K., Carbone, F.R., et al. (2009). Cross-presentation of viral and self antigens by skin-derived CD103+ dendritic cells. Nat. Immunol. *10*, 488–495. https://doi.org/10.1038/ni.1724.
56. Naik, S.H., Proietto, A.I., Wilson, N.S., Dakic, A., Schnorrer, P., Fuchsberger, M., Lahoud, M.H., O'Keeffe, M., Shao, Q.X., Chen, W.F., et al. (2005). Cutting edge: generation of splenic CD8+ and CD8- dendritic cell equivalents in Fms-like tyrosine kinase 3 ligand bone marrow cultures. J. Immunol. *174*, 6592–6597. https://doi.org/10.4049/jimmunol.174.11.6592.
57. Liao, Y., Smyth, G.K., and Shi, W. (2013). The Subread aligner: fast, accurate and scalable read mapping by seed-and-vote. Nucleic Acids Res. *41*, e108. https://doi.org/10.1093/nar/gkt214.
58. Liao, Y., Smyth, G.K., and Shi, W. (2014). featureCounts: an efficient general purpose program for assigning sequence reads to genomic features. Bioinformatics *30*, 923–930. https://doi.org/10.1093/bioinformatics/btt656.
59. Robinson, M.D., and Oshlack, A. (2010). A scaling normalization method for differential expression analysis of RNA-seq data. Genome Biol. *11*, R25. https://doi.org/10.1186/gb-2010-11-3-r25.
60. Ritchie, M.E., Phipson, B., Wu, D., Hu, Y., Law, C.W., Shi, W., and Smyth, G.K. (2015). limma powers differential expression analyses for RNA-sequencing and microarray studies. Nucleic Acids Res. *43*, e47. https://doi.org/10.1093/nar/gkv007.
61. Law, C.W., Chen, Y., Shi, W., and Smyth, G.K. (2014). voom: Precision weights unlock linear model analysis tools for RNA-seq read counts. Genome Biol. *15*, R29. https://doi.org/10.1186/gb-2014-15-2-r29.
62. Phipson, B., Lee, S., Majewski, I.J., Alexander, W.S., and Smyth, G.K. (2016). Robust Hyperparameter Estimation Protects against Hypervariable Genes and Improves Power to Detect Differential Expression. Ann. Appl. Stat. *10*, 946–963. https://doi.org/10.1214/16-AOAS920.
63. McCarthy, D.J., and Smyth, G.K. (2009). Testing significance relative to a fold-change threshold is a TREAT. Bioinformatics *25*, 765–771. https://doi.org/10.1093/bioinformatics/btp053.
64. Wu, D., Lim, E., Vaillant, F., Asselin-Labat, M.L., Visvader, J.E., and Smyth, G.K. (2010). ROAST: rotation gene set tests for complex microarray experiments. Bioinformatics *26*, 2176–2182. https://doi.org/10.1093/bioinformatics/btq401.
65. Morelli, A.E., Larregina, A.T., Shufesky, W.J., Zahorchak, A.F., Logar, A.J., Papworth, G.D., Wang, Z., Watkins, S.C., Falo, L.D., Jr., and Thomson, A.W. (2003). Internalization of circulating apoptotic cells by splenic marginal zone dendritic cells: dependence on complement receptors and effect on cytokine production. Blood *101*, 611–620. https://doi.org/10.1182/blood-2002-06-1769.

## STAR★METHODS

### KEY RESOURCES TABLE

| REAGENT or RESOURCE | SOURCE | IDENTIFIER |
|---|---|---|
| Antibodies | | |
| Fixable Viability Dye (FVD) eFluor 780 | eBioscience | Cat# 65-0865-18 |
| Anti-mouse CD45.1-FITC, Clone A20 | Biolegend | Cat# 110706; RRID:AB_313495 |
| Anti-mouse CD8α-PE-Cy7, Clone 53–6.7 | Biolegend | Cat# 100722; RRID:AB_312761 |
| Anti-mouse CD8α-BV421, Clone 53–6.7, 100738, Biolegend | Biolegend | Cat# 100738; RRID:AB_11204079 |
| Anti-mouse CD4-APC, Clone GK1.5 | WEHI mAb facility | N/A |
| Anti-mouse TCRVα2-FITC, Clone B20.1 | WEHI mAb facility | N/A |
| Anti-mouse TCRVb5.1, 5.2-PE, Clone MR9-4 | Biolegend | Cat# 139504; RRID:AB_10613279 |
| Anti-mouse CD45-BV786, Clone 30-F11 | BD Biosciences | Cat# 564225; RRID:AB_2716861 |
| Anti-mouse CD45.1-APC, Clone A20.1 | WEHI mAb facility | N/A |
| Anti-mouse CD45.1-PE-Cy7, Clone A20 | eBioscience | Cat# 25-0453-82; RRID:AB_469629 |
| Anti-mouse CD45RA-FITC, Clone OX-33 | Biolegend | Cat# 202305; RRID:AB_314009 |
| Anti-mouse CD11c-BV711, Clone N418 | Biolegend | Cat# 117349; RRID:AB_2563905 |
| Anti-mouse I-A/I-E (panMHC II)-BV421, Clone M5/114.15.2 | Biolegend | Cat# 107632; RRID:AB_2650896 |
| Anti-mouse CD172a (Sirpα)-AF700, Clone P84 | Biolegend | Cat# 144022; RRID:AB_2650813 |
| Anti-mouse CD11b-APC, Clone M1/70 | WEHI mAb facility | N/A |
| Anti-mouse CD11b-BV510, Clone M1/70 | Biolegend | Cat# 101263; RRID:AB_2629529 |
| Anti-mouse XCR1-BV650, Clone ZET | Biolegend | Cat# 148220; RRID:AB_2566410 |
| Anti-mouse CD24-PE, Clone 30-F1 | Biolegend | Cat# 138504; RRID:AB_10578416 |
| Anti-mouse DEC205-PE, clone NLDC-145 | WEHI mAb facility | N/A |
| Anti-mouse CD80-FITC, Clone 16-10A1 | WEHI mAb facility | N/A |
| Anti-mouse CD86-BV650, Clone GL-1 | Biolegend | Cat# 105035; RRID:AB_11126147 |
| Anti-mouse CD40-PE, Clone 3/23 | Biolegend | Cat# 124610; RRID:AB_1134075 |
| Anti-mouse CD103-PE, Clone 2E7 | Biolegend | Cat# 121406; RRID:AB_1133989 |
| Anti-mouse CD207 (Langerin)-PE, Clone 4C7 | Biolegend | Cat# 144204; RRID:AB_2561499 |
| Anti-mouse CD1d-A488, Clone 1B1 | eBioscience | Cat# 53-0011-80; RRID:AB_1944358 |
| Anti-mouse Ly-6A/E (Sca-1)-APC, Clone D7 | Biolegend | Cat# 108112; RRID:AB_313349 |
| Anti-mouse TGFbRII-Fluorescein | R & D systems | Cat# FAB532F; RRID:AB_10645653 |
| Anti-mouse CD124 (IL-4Rα)-APC, Clone I015F8 | Biolegend | Cat# 144804; RRID:AB_2561730 |
| Anti-mouse CD210 (IL-10R)-PE, Clone 1B1.3α | BD Biosciences | Cat# 559914; RRID:AB_397369 |
| Anti-mouse CD120b (TNFRSF1b)-PE, Clone TR75-89 | Biolegend | Cat# 113405; RRID:AB_2206942 |
| Anti-mouse CD137 (TNFRSF9)-PE, Clone 17B5 | Biolegend | Cat# 106105; RRID:AB_2205693 |
| Anti-mouse CD134 (OX-40) TNFRSF4-PE, Clone OX-86 | Biolegend | Cat# 119410; RRID:AB_2207344 |
| Anti-mouse Siglec-2 (CD22)-APC, Clone 308501 | R & D systems | Cat# FAB2296A; RRID:AB_2074566 |
| Anti-mouse CD81-APC, Clone Eat-2 | Biolegend | Cat# 104909; RRID:AB_2562993 |
| Anti-mouse CD184 (CXCR4)-PE, Clone 2B11 | eBioscience | Cat# 12-9991-81; RRID:AB_891393 |
| Anti-mouse IRF4-eFluor660, Clone 3E4 | eBioscience | Cat# 50-9858-82; RRID:AB_2574393 |
| Anti-mouse IRF7-PE, Clone MNGPKL | eBioscience | Cat# 12-5829-80; RRID:AB_2572628 |
| Anti-mouse CD3Ɛ, Clone KT3-1.1 | WEHI mAb facility | N/A |
| Anti-mouse Thy1, Clone T24/31.7 | WEHI mAb facility | N/A |
| Anti-mouse B220, Clone RA3-6B2 | WEHI mAb facility | N/A |
| Anti-mouse Gr1, Clone RB6-8C5 | WEHI mAb facility | N/A |

(*Continued on next page*)

*Continued*

| REAGENT or RESOURCE | SOURCE | IDENTIFIER |
|---|---|---|
| Anti-mouse erythrocyte, Clone TER-119 | WEHI mAb facility | N/A |
| Anti–DEC205-OVA, Clone NLDC145-OVA | From M. Lahoud | N/A |
| rat IgG2a isotype control mAb-OVA, Clone GL117-OVA | From M. Lahoud | N/A |
| Anti-Clec9A–$OVA_{FGD}$–A647 | From W.R. Heath | N/A |
| isotype–$OVA_{FGD}$–A647 | From W.R. Heath | N/A |
| Anti-Clec9A-Eα peptide, Clone 10B4 | From I. Caminschi | N/A |
| isotype-Eα peptide | From I. Caminschi | N/A |
| Anti-mouse TGFβ blocking mAb, Clone 1B11 | WEHI mAb facility | N/A |
| rat IgG1κ isotype control | WEHI mAb facility | N/A |
| LEAF purified anti-mouse CD210 (IL-10R), Clone 1B1.3a | Biolegend | CAT# 112708; RRID:AB_313521 |
| LEAF purified rat IgG1κ isotype control, Clone RTK2071 | Biolegend | CAT# 400414; RRID:AB_326520 |
| **Bacterial and virus strains** | | |
| Plasmodium berghei ANKA strain | Lundie et al.[28] | N/A |
| Influenza A virus | Jenkins et al.[48] | x31-OVA |
| Herpes simplex virus (HSV)-1 | Gift from L. Brown, University of Melbourne | N/A |
| **Chemicals, peptides, and recombinant proteins** | | |
| bromodeoxyuridine (BrdU) | Sigma-Aldrich | 19160 |
| CpG1668 (20mer) 5′-T*C*C*A*T*G*A*C*G*T*T*C*C*T*G*A*T*G*C*T | Bioneer | N/A |
| LPS from Escherichia coli O127:B8 | Sigma-Aldrich | L3129 |
| Poly(I:C) HMW | InvivoGen | tlrl-pic-5 |
| Chloroquine | Sigma-Aldrich | 6823-83-2 |
| Hoechst 33258 solution | ThermoFisher Scientific | H3569 |
| FACS buffer (PBS 2% FCS) | Made in-house | N/A |
| Albumin from chicken egg white, lyophilized powder, ≥98% | Sigma-Aldrich | A5503-10G |
| Ovalbumin egg white purified | Worthington | LS003054 |
| RPMI 1640 medium | Made in-house | N/A |
| penicillin-streptomycin | made in-house | N/A |
| Glutamax | Gibco | 35050061 |
| 2-mercaptoethanol | Gibco | 21985023 |
| Streptavidin Fluoresbrite YG microspheres (1.0 μm in diameter) | Polysciences | 24161–5 |
| Fluoresbrite YG carboxylate microspheres (0.5 μm) | Polysciences | 15700–10 |
| PKH26 red fluorescent cell linker kit for general cell membrane labeling | Sigma-Aldrich | PKH26GL-1KT |
| OVA-biotin | Worthington | Worthington |
| Ovalbumin, fluorescein conjugate | ThermoFisher | O23020 |
| Nycodenz | Nycomed Pharma | N/A |
| Recombinant murine FLT3 ligand | PeproTech | 250-31L |
| Neomycin sulfate | Enzo Life Sciences | ALX-380-035 |
| Sphero blank calibration particles 6.0–6.4 um | BD Biosciences | 556396 |
| Anti-Clec9A-YAe | Made at-house | N/A |
| Biotinylated anti-mouse Eα52-68 (clone eBioYAe) | eBioscience | 13–5741 |
| BioMag goat anti-rat IgG | Qiagen | 310107 |

(*Continued on next page*)

*Continued*

| REAGENT or RESOURCE | SOURCE | IDENTIFIER |
|---|---|---|
| Paraformaldehyde 16% solution, EM grade | Electron Microscopy Sciences | 15710 |
| Sucrose | Chem-Supply | SA030 |
| Dako protein block serum-free | Agilent | X0909 |
| ProLong Gold antifade mountant | ThermoFisher | P36930 |
| NEB 100 bp ladder | BioLabs New England | N0467L |
| DirectPCR Lysis Reagent (Mouse Tail) | Viagen | 102-T |
| Proteinase K, recombinant, PCR grade | Roche | 3115879001 |
| GoTag Green master mix | Promega | M7123 |
| Agarose molecular grade | Bioline | Bio-41025 |
| SYBR Safe DNA gel stain | Invitrogen | S33102 |
| Collagenase type 3 | Worthington | LS004183 |
| DNase I (Deoxyribonuclease I) | Roche | 10104159001 |
| EDTA | Sigma-Aldrich | E5134 |
| RBC lysis buffer | Made in-house | N/A |
| Bovine Serum Albumin (BSA) | Sigma | A7906 |
| GolgiPlug | BD Biosciences | 555029 |
| Propidium iodide | ThermoFisher | P1304MP |
| Cytochalasin D | Gibco | PHZ1063 |
| Cytochrome *c* from equine heart | Sigma-Aldrich | C7150 |
| **Critical commercial assays** | | |
| CBA mouse inflammation kit | BD Bioscience | 552364 |
| Mouse Th1/Th2/Th17 CBA kit | BD Bioscience | 560485 |
| BD Cytofix/Cytoperm kit | BD Bioscience | 554714 |
| CellTrace$^{TM}$ Violet Cell Proliferation Kit | Invitrogen | C34557 |
| CellTrace CFSE Cell Proliferation Kit | Invitrogen | C34554 |
| RNeasy plus mini-kit | QIAGEN | 74034 |
| SuperScript III First-strand synthesis system | Thermofisher scientific | 18080051 |
| **Deposited data** | | |
| RNA-seq data | This paper | GEO: GSE68697; GEO: GSE207845 |
| **Experimental models: Cell lines** | | |
| Murine Flt3L secreting B16 melanoma cell line | Segura et al.[49] | N/A |
| **Experimental models: Organisms/strains** | | |
| Mouse: C57BL/6J (B6) | The Jackson Laboratory | JAX: 000664 |
| Mouse: B6.SJL-Ptprc$^{a}$Pep3$^{b}$/BoyJ (CD45.1) | Charles River | N/A |
| Mouse: mutant B6.C-H-2$^{bm1}$ (bm1) | Nikolić-Zugić et al.[50] | N/A |
| Mouse: C57/B6.129S2-H2$^{dlAb1-Ea}$/J (H2) | The Jackson Laboratory | JAX: 003584 |
| Mouse: B6-Tg(TcraTcrb)1100Mjb/J (OT-I) | Hogquist et al.[51] | N/A |
| Mouse: B6.Cg-Tg(TcraTcrb)425Cbn/J (OT-II) | Barnden et al.[52] | N/A |
| Mouse: Tg(TcraHsv2.3,TcrbHsv2.3)L118-1Cbn (gBT-I) | Mueller et al.[53] | N/A |
| Mouse: CD11c-mOVA | Wilson et al.[23] | N/A |
| Mouse: B6.129-Pparg$^{tm2Rev}$/J (PPAR$\gamma^{loxP}$) | The Jackson Laboratory | JAX:004584 |
| Mouse: B6.Cg-Tg(Itgax-Cre)1-1Reiz/J (Itgax-Cre) | The Jackson Laboratory | JAX:008068 |
| Mouse: C57BL/6J-Tlr9$^{M7Btlr}$/Mmjax (TLR9$^{-/-}$) | The Jackson Laboratory | JAX: 34329 |
| Mouse: Tgfb2r$^{fl/fl}$ | Ramalingam et al.[41] | N/A |
| **Oligonucleotides** | | |
| Ppar$\gamma^{fl/fl}$ Fwd 5′-TGGCTTCCAGTGCATAAGTT-3′ | Bioneer | N/A |
| Ppar$\gamma^{fl/fl}$ Rev 5′-TGTAATGGAAGGGCAAAAGG-3′ | Bioneer | N/A |
| CD11cCre Fwd-1 5′-ACTTGGCAGCTGTCTCCAAG-3′ | Bioneer | N/A |

(*Continued on next page*)

| Continued | | |
|---|---|---|
| REAGENT or RESOURCE | SOURCE | IDENTIFIER |
| CD11cCre Fwd-2 5′-CAAATGTTGCTTGTCTGGTG-3′ | Bioneer | N/A |
| CD11cCre Rev-1 5′-GCGAACATCTTCAGGTTCTG-3′ | Bioneer | N/A |
| CD11cCre Rev-2 5′-GTCAGTCGAGTGCACAGTTT-3′ | Bioneer | N/A |
| Software and algorithms | | |
| FlowJo v10.5.3 | FlowJo, LLC | RRID:SCR_008520 |
| Prism 8 | GraphPad | RRID:SCR_002798 |
| Adobe Illustrator CC 2022 | Adobe | https://www.adobe.com/ |
| R | R Project for Statistical Computing | RRID:SCR_001905 |
| R packages Rsubread, limma and edgeR | Bioconductor 3.1 | RRID:SCR_006442 |
| FCAP Array v3.0.1 | BD Biosciences | Cat# 652099 |
| ImageJ | National Institutes of Health | N/A |
| Zen Black software | Zeiss | N/A |
| Other | | |
| FACS Canto II | BD Biosciences | N/A |
| LSR-II | BD Biosciences | N/A |
| FACSAria III | BD Biosciences | N/A |
| Cryostat | Leica Biosystems | N/A |
| Zeiss LSM 780 scanning confocal microscope | Zeiss | N/A |
| Veriti thermal cycler | Thermofisher scientific | Cat# 4375305 |
| GelDoc system | Bio-Rad | N/A |

## RESOURCE AVAILABILITY

### Lead contact

Further information and requests for resources and reagents should be directed to and will be fulfilled by the lead contact, Jose Villadangos (J.villadangos@unimelb.edu.au).

### Materials availability

This study did not generate new unique reagents.

### Data and code availability

All data is available in the main text or the supplementary materials. The RNA-seq data has been uploaded to the GEO repository (GEO: GSE68697; GEO: GSE207845). Any additional information required to reanalyze the data reported in this paper is available from the lead contact upon request.

## EXPERIMENTAL MODEL AND STUDY PARTICIPANT DETAILS

### Mice

The mice used were C57BL/6J (B6), B6.SJL-*Ptprc*$^{a}$*Pep3*$^{b}$/BoyJ (CD45.1), mutant B6.C-H-2$^{bm1}$ (bm1),[50] B6.*129S2-H2*$^{dlAb1\text{-}Ea}$/J (H2) (knock out for MHC-II gene, MHC II$^{-/-}$), B6-Tg(*TcraTcrb)1100Mjb*/J (OT-I),[51] B6.Cg-*Tg(TcraTcrb)425Cbn*/J (OT-II),[52] Tg(*TcraHsv2.3,TcrbHsv2.3)L118-1Cbn* (gBT-I),[53] CD11c-mOVA (membrane OVA is expressed under the control of *Itgax* promoter),[23] B6.129-*Pparg*$^{tm2Rev}$/J (*PPARγ*$^{loxP}$) crossed to B6.Cg-Tg(*Itgax*-Cre)1-1Reiz/J (in which Cre recombinase is expressed under the control of the *Itgax* promoter, so-called *Itgax*-Cre mice), C57BL/6J-*Tlr9*$^{M7Btlr}$/Mmjax (*TLR9*$^{-/-}$), *Tgfb2r*$^{fl/fl}$ (floxed regions around *Tgfb2r* gene)[41] crossed to *Itgax*-Cre mice. Both male and female mice were used. All mice were maintained in specific pathogen-free (SPF) conditions at the Bio21 Institute Animal Facility (Parkville, Australia) following institutional guidelines and were used between six and 16 weeks of age. Experimental procedures were approved by the Animal Ethics Committee of the University of Melbourne (Ethics no. 1714375, 20088).

## METHOD DETAILS

### Induction of systemic inflammatory response syndrome

Where indicated, mice were injected intravenously (*i.v.*) in the tail vein with 0.4, 1.25, 2.3, 5, 7 or 20 nmol of synthetic CpG1668, or 10 μg of LPS, dissolved in 200 μL of PBS. The malaria-cured infection was induced by *i.v.* injection of $10^{6}$ *Plasmodium berghei* ANKA

strain (PbA)-parasitized red blood cells followed by intraperitoneal (*i.p.*) injection of 0.4 mg chloroquine daily from day 4 to day 8, and 600 mg/L chloroquine in drinking water on day 9 and day 10 as described.[29] Parasitaemia was quantified in giemsa-stained thin blood smears on indicated days.

### Induction and monitoring of blood stage malaria infection

Mice were *i.v.* infected with $10^6$ blood stage PbA parasites diluted in 200 μL sterile PBS. After infection, mice were *i.p.* injected with 0.8 mg chloroquine dissolved in PBS daily from day 4–8, followed by 600 mg/L chloroquine in drinking water on days 8–10, as shown in Figure S1H. Parasitemia was assessed by microscopic analysis of blood smears or by flow cytometry, by incubating ~2 μL tail blood with a 5 pg/mL Hoechst 33258 solution in FACS buffer for 1 h at 37°C. Parasites were discriminated from uninfected RBC using a 405 violet laser and a 450/50 filter.

### Cytokine profiling in sera and culture supernatants

Mice were injected *i.v.* with different doses of CpG, 10 μg of LPS or were infected-cured with PbA-CQ. Blood was collected in Eppendorf tubes and incubated on ice for 6 h, before centrifugation at 7000*g* for 5 min. The sera were transferred into fresh tubes and stored at −20°C until examination. Flow cytometry-based cytometric bead array mouse inflammation CBA kit was used to analyze cytokine concentrations in mouse sera or in supernatant of DC cultures. The assay was performed as per the kit manufacturer protocol, and beads were run on a FACS Canto II. Standard curves and concentration of cytokines were calculated using FCAP Array v3.0.1 as per the manufacturer's instructions.

### Preparation of CellTrace violet-labeled T-cells

OT-I cells (H-$2^b$-restricted anti-$OVA_{257–264}$), gBT-I cells (H-$2K^b$-restricted anti-HSV $gB_{498–505}$), or OT-II cells (H-$2^b$-restricted anti-$OVA_{323–339}$) were purified from pooled lymph nodes (inguinal, axillary, brachial, sacral, cervical and mesenteric) of transgenic Ly5.$1^+$ mice by depletion of non-$CD8^+$ T-cells, and were labeled with CellTrace Violet (CTV) as described previously.[23] T cell preparations were routinely 85–95% pure, as determined by flow cytometry. In order to transfer OT-cells to B6 mice, donors with genotype of Cg/Cg (phenotype of CD45.1+ CD45.2-) were used. To transfer OT-cells to chimeric mice, donors with genotype of Cg/+ (phenotype of CD45.1+ CD45.2+) were used.

### Preparation of cell-associated OVA

To prepare OVA-coated splenocytes (OCS), splenocytes from bm-1 or MHC $II^{-/-}$ mice were incubated for 10 min at 37°C with 10 mg/mL of albumin from chicken egg white (OVA) in RPMI 1640 medium, were irradiated with 1,500 cGy, and were washed 3 times in RPMI 1640 medium with 2% FCS before injection.

### Preparation of fluorescent OVA-coated beads (OCB)

Streptavidin Fluoresbrite YG microspheres (1.0 μm) were incubated with equal volume of biotinylated OVA for 30 min at 4°C. Beads were washed at 10000 g for 6 min and incubated with FCS at 37°C water bath for 1 h. 1.5 x $10^9$ (in 100 μl) beads/mouse were *i.v.* injected, or 2 x $10^8$ (5.5 μl) OCB per 1 x $10^6$ cDC were incubated *in vitro*.

### Priming of OT-cells *in vivo*

Mice were injected *i.v.* with 2 x $10^6$ CTV-labeled OT-I or OT-II cells. One day later, mice were injected *i.v.* with 20 x $10^6$ OCS, or 0.1 mg of soluble OVA with or without LPS (0.4 μg/mouse), or 0.5 μg of anti-DEC205-OVA (clone NLDC-45).[34] Sixty hours later, total splenocytes were stained with the following conjugated monoclonal antibodies (mAb): Fixable Viability Dye (FVD) eFluor 780, CD45.1-FITC, CD8α-PE-Cy7 (for OT-I); CD4-APC (for OT-II). To stain for OT-cells in chimeric mice, FVD eFluor 780, TCRVα2-FITC, TCRVb5.1, 5.2-PE, CD45.2-BV786. Also, for OT-I; CD8α-PE-Cy7, CD45.1-APC, and for OT-II; CD4-APC; CD45.1-PE-Cy7. Cells were resuspended in buffer containing 2.5 x $10^4$ blank calibration particles. Samples were acquired on an LSR-II and analyzed using FlowJo software. Total number of live dividing OT-cells ($CTV^{low}$) was calculated per spleen.

### *In vivo* CTL assay

Suspensions of a mixture of splenocytes and lymph node cells from B6 mice were depleted of red blood cells and split into two equal portions. One was pulsed for 1 h at 37°C with 0.1 mg/mL of $OVA_{257–264}$ and then labeled with a high concentration (2.5 mM) of CFSE ($CFSE^{hi}$ population). The other was incubated for 1 h at 37°C without peptide and was labeled with a low concentration (0.25 mM) of CFSE ($CFSE^{low}$ population). Equal numbers of cells from each population were combined and 20 x $10^6$ cells were transferred by *i.v.* injection. Cell suspensions from spleen and peripheral lymph nodes (of inguinal, axillary, and brachial) were analyzed 4 h later by flow cytometry. The percent of OVA lysis was determined by the loss of the peptide-pulsed $CFSE^{hi}$ population compared with the control $CFSE^{low}$ population.[54]

### Presentation of viral antigens after CpG

Untreated mice or mice pretreated with CpG or PbA infected-cured mice were subsequently infected at indicated days with HSV-1 (2 x $10^5$ plaque-forming units (PFU)/mouse *i.v.*, a gift from L. Brown, University of Melbourne, Melbourne, Australia). Mice were

injected *i.v.* separately with 1 x $10^6$ CTV-labeled gBT-I. After 60 h, gBT-I proliferation in spleen was determined by flow cytometry. To measure the endogenous anti-HSV response, seven days after infection spleens were collected and the percentage of $K^b$-gB$^+$ CD8$^+$ T-cells was determined by flow cytometry as previously described.[55]

### BrdU incorporation

Mice were injected *i.p.* with 1 mg bromodeoxyuridine (BrdU) in saline and then were continuously given BrdU (0.8 mg/mL) in sterile drinking water that was changed daily. After 5 days, DCs were isolated and analyzed as described previously.[19]

### Preparation of single cells from spleen

Spleens were chopped and digested by resuspension for 20 min at room temperature (RT) in RPMI 1640 medium with 2% FCS and 0.7 mg/mL of collagenase type 3 and 0.1 mg/mL of DNase I. EDTA (final 10 mM) was then added and resuspended for further 5 min at RT. The suspension was passed through 70 μm strainer.

### cDC isolation, analysis and culture

DC purification from spleen, analytical and preparative flow cytometry and DC cultures *in vitro* were performed as described previously.[19] The following conjugated monoclonal antibodies were used: FVD eFluor 780; CD45RA-FITC, CD11c-BV711, I-A/I-E (panMHC II)-BV421, CD8α-PE-Cy7; CD172a (Sirpα)-AF700, CD11b-APC, XCR1-BV650, CD24-PE, DEC205-PE, CD11b-BV510, and CD8α-BV421. Activation and paralysis markers: CD80-FITC, CD86-BV650, CD40-PE, 3/23, CD103-PE, CD207 (Langerin)-PE, CD1d-A488, Ly-6A/E (Sca-1)-APC, TGFbRII-Fluorescein, CD124 (IL-4Rα)-APC, CD210 (IL-10R)-PE, CD120b (TNFRSF1b)-PE, CD137 (TNFRSF9)-PE, CD134 (OX-40) TNFRSF4-PE, Siglec-2 (CD22)-APC, CD81-APC, CD184 (CXCR4)-PE, IRF4-eFluor660, and IRF7-PE. Samples were acquired on an LSR-Fortessa and analyzed using Flowjo software. When necessary, DC obtained from the spleen of 2–10 mice were pooled and sorted with a FACSAria III (purity >95%). The cells were subsequently used for cell culture or analysis of RNA. DC were generated from bone marrow precursors in culture medium supplemented with Fms-like tyrosine kinase 3 (Flt3) ligand (Flt3L) as previously described.[56]

### RNA-seq expression profiling

Cells were FACS sorted (on average 3.5 x $10^6$ cells per sample with purity over 95%) by using gating strategy as shown in Figure S1D; cDC1 were gated as CD11c+CD45RA- > CD11b-CD8α+, cDC2 were gated as CD11c+CD45RA- > CD11b+CD8α-. Cells were lysed for RNA preparation using the QIAGEN RNeasy plus mini-kit. RNA yields of 5 μg or above were used for sequencing. Two independent RNA samples were obtained from paralyzed CD103$^{high}$ and from untreated CD103$^{low}$ CD8α+ cDC (cDC1). Three independent RNA samples were obtained from untreated CD103$^{neg}$ cDC1, and from untreated cDC2 or paralyzed cDC2. RNA samples were sequenced at the Beijing Genomics Institute using Illumina HiSeq 2000 sequencing systems. Reads were aligned to the to the mm10 mouse genome using Subread v1.4.6.[57] Reads counts were obtained using featureCounts[58] and Rsubread's inbuilt RefSeq annotation.

Differential expression analyses were performed using the Bioconductor packages edgeR[59] and limma.[60] Ribosomal and immunoglobin genes were filtered, as were low abundance genes with average log-count-per-million less than zero. Library sizes were normalized by the TMM method.[59] Counts were transformed to log2-counts per million (logCPM) with associated precision weights using voom.[61] Differential expression between the cell populations as assessed using empirical Bayes moderated t and F-statistics, with robust estimation of the Bayesian hyper-parameters.[60,62] The cDC2 linear model was undertaken as a paired analysis. The paralyzed cDC1 population was compared to the average of the two untreated cDC1 populations using a linear model contrast. In order to restrict attention to genes showing biological meaningful expression changes, genes were only considered to be differentially expressed if the fold change was significantly greater than 1.5 using the TREAT method.[63] The Benjamini and Hochberg method was used to control the TREAT false discovery rate (FDR) below 10%. A TREAT of 0.1 corresponds to a conventional FDR of less than 0.05.

A rotation gene set test (ROAST) was used to compare the average expression of cDC1 markers in paralyzed cDC1 vs. the two untreated cDC1, and also the average expression of cDC2 markers in paralyzed cDC2 vs. untreated cDC2.[64] Heatmaps show log2-counts-per-million computed by edgeR's cpm function.

### Cytochrome C-induced depletion of cross-presenting cDC1

Mice were *i.v.* injected twice with 5 mg of horse cytochrome *c* with an interval of 12 h. 12 h after the second injection, DC were purified and quantitated as described previously.[32]

### *In vitro* phagocytosis assays

Enriched cDC were seeded in flat-bottom 12 well plate in complete DC medium; RPMI 1640 medium, 10% FCS, 1% penicillin-streptomycin, 1% Glutamax, and 0.2% 2-mercaptoethanol. Fluorescent OCB were added at numbers indicated earlier, for 3–4 h at 37°C. DC were then stained with FVD eFluor 780 and for surface markers. The frequencies of phagocytic DC were determined by flow cytometry as percentages of OCB+ cells among cDC1 and cDC2.

### *In vivo* endocytosis and phagocytosis assays

Mice were injected *i.v.* with 1 mg of OVA-fluorescein (for 45 min), 3.64 x $10^9$ Fluoresbrite YG carboxylate microspheres (0.5 mm in diameter) (for 2 h), 1.5 x $10^9$ fluorescent OCB (for 2 h), or 20 x $10^6$ PKH26+ OCS (for 2 or 12 h). After the indicated durations, spleens were harvested, and uptake of antigen was assessed by flow cytometry as described previously.[23,65]

### Intracellular staining of cytokines

Enriched cDC were cultured for 8 h in complete DC medium in the presence of 1 μl/ml GolgiPlug, and were stained with FVD eFluor 780 and for surface markers in the presence of GolgiPlug. Fixation and permeabilization were performed by use of BD Cytofix/Cytoperm Fixation/Permeabilization kit, following manufacturer instructions. Fixed and permeabilized cells were incubated with mAb for cytokines or isotype controls for 2–3 h on ice, and were read by flow cytometry.

### *ex vivo* priming of OT-cells

Following *in vivo* endocytosis or phagocytosis, at time-points indicated above, spleens were harvested and cDC were enriched, and stained for surface markers. Endocytic/phagocytic or non-endocytic/non-phagocytic cDC1 and cDC2 were FACS-sorted and cultured in U-bottom 96 well plate (10 x $10^3$ to 25 x $10^3$ DC/200ul complete DC medium/well). 25 x $10^3$ CTV-labeled OT-cells/well were added. Proliferation was assessed after 60–70 h of incubation.

### Spleen confocal fluorescence microscopy

Spleens were fixed in 4% paraformaldehyde for 3 h, incubated in 30% sucrose overnight and cryofreezed by liquid nitrogen. Sections of 16 or 70 μm thickness were prepared by use of Cryostat. The 70 μm sections, after 30 min of drying out at RT, were directly used for examination with fluorescence confocal microscope. The sections of 16 μm thickness, after 30 min of drying out at RT, were blocked by Dako block, then counterstained with appropriate primary and secondary antibodies. The slides were subsequently mounted with ProLong Gold antifade mountant. Imaging was performed using the Zeiss LSM 780 scanning confocal microscope. All images were analyzed using ImageJ or Zen Black software.

### Generation of full or mixed bone marrow chimeras

Bone marrow (BM) was obtained from tibia and femur bones of donor mice after flushing by use of 25G needles. Recipient mice were γ-irradiated twice with 550 Gy and were reconstituted with 5 x $10^6$ BM cells for full chimeras, or 2.5 x $10^6$ BM cells of each donor strain for 1:1 mixed chimeras, or 1.7 x $10^6$ and 3.3 x $10^6$ BM cells of each relevant donor strain for 1:2 mixed chimeras. Neomycin (50 mg/mL) was added to the drinking water for the following 3 weeks. Chimeras were used for subsequent experiments after 8 weeks of reconstitution. The percentage of chimerism was tested before or during the experiments.

### Enrichment of CD11cint cells

Spleens were mechanically and enzymatically digested. Supernatant after centrifugation of splenocytes in isosmotic nycodenz medium of 1.077 g/$cm^3$ density was sampled as "before depletion", then used for negative enrichment by use of cDC mAb enrichment cocktail as described before.[19] Cells of non-cDC lineage were depleted by incubating the cells in an antibody cocktail comprising anti-CD3Ɛ (KT3-1.1), anti-Thy1 (T24/31.7), anti-B220 (RA3-6B2), anti-Gr1 (RB6-8C5), and anti-erythrocyte (TER-119), then removing the Ab-binding cells with goat anti-rat IgG magnetic beads.

### Late stage pre-DC cells

B6 mice were injected subcutaneously with 5 x $10^6$ B16 melanoma cells secreting murine Flt3L and euthanized after 9–10 days.[49] Pre-DC ($CD11c^{high}CD24^{high}CD8\alpha^{neg}CD11b^{neg}$) were collected from the spleen by negative selection as described previously.[38]

### Cell transfer to non-irradiated mice

For BM cells transfer, 20 x $10^6$ per recipient was transferred (experimental designs in Figure S4B). The average number of cDC derived from the transferred cell ±SEM was 0.062 ± 0.09 in unpretreated recipients and 0.048 ± 0.0.9 in CpG-pretreated recipients. For $CD11c^{int}$ cell and cDC transfer, 0.5-1 x $10^6$ per recipient was transferred (experimental designs in Figures S4D and S4F).

### Induction of influenza A virus pulmonary infection

$10^4$ PFU of influenza virus H3N2A-x31 with OVA peptide$^{257-264}$ SIINFEKL inserted into neuraminidase stalk; x31-OVA as described in,[48] diluted in 50 μl sterile PBS, was inoculated intranasally to anesthetized mice to induce a non-lethal acute pneumonia.

### PCR for genotyping *Itgax*-Cre and *PPARγ*$^{fl/fl}$ mice

Total DNA was prepared by heating mouse earclips or FACS-sorted cDC in mouse tail DirectPCR lysis buffer and proteinase K at final concentration of 0.3 mg/mL at 55°C overnight, followed by 45 min at 85°C. The supernatant was used as template DNA. Primers used are noted in key resources table. Primers and GoTaq Green master mix were used in PCR reaction which was run in Veriti thermal cycler. PCR products were run on 2% agarose gel containing 1:1000 of SYBR Safe, along with 100 bp DNA ladder for 30 min at 120 V. Gels were visualized in GelDoc system.

### Antibodies used for targeting and blocking

Anti–DEC205-OVA or rat IgG2a isotype control mAb-OVA were obtained from A/Prof. Mireille Lahoud laboratory. 0.5 μg was *i.v.* injected per mouse. Anti-Clec9A–$OVA_{FGD}$–A647 and isotype–$OVA_{FGD}$–A647 were obtained from Prof. William Heath laboratory. 2 μg was *i.v.* injected per mouse. Anti-Clec9A-Eα peptide and isotype-Eα peptide were obtained from A/Prof. Irina Caminschi laboratory. 5 μg was *i.v.* injected per mouse. TGFβ blocking mAb and rat IgG1κ isotype control were purchased from WEHI mAb facility. 44 μg was *i.p.* injected per injection/mouse. CD210 (IL-10R) blocking mAb and rat IgG1κ isotype control were purchased from Biolegend were *i.p.* injected (150 μg/mouse/2 days).

## QUANTIFICATION AND STATISTICAL ANALYSIS

Data were plotted using GraphPad prism. Independent-samples t test with Welch's correction (no assumption of equal variances) followed by Dunnett's T3 multiple comparisons test were used for statistical analyses. Statistical details of experiments (number of mice per group and p values) can be found in the figure legends. Bars in graphs denote mean ± SE. $p \leq 0.05$ for statistical significance. Blank or ns: non-significant, *$p \leq 0.05$ **$p \leq 0.01$, ***$p \leq 0.001$, ****$p \leq 0.0001$ [two-tailed p value (95% CI)].